

A three-scale model of spatio-temporal bursting

Abstract

We study spatio-temporal bursting in a three-scale reaction diffusion equation organized by the winged cusp singularity. For large time-scale separation the model exhibits traveling bursts, whereas for large space-scale separation the model exhibits standing bursts. Both behaviors exhibit a common singular skeleton, whose geometry is fully determined by persistent bifurcation diagrams of the winged cusp. The modulation of spatio-temporal bursting in such a model naturally translates into paths in the universal unfolding of the winged-cusp.

1 Introduction

In the recent paper [1], we proposed that temporal bursting can be conveniently studied in a three-time-scale model with a single scalar *winged-cusp* nonlinearity, a basic organizing center in the language of singularity theory. Because of its particular structure, the model is readily interpreted as a three-scale generalization of the celebrated Fitzgugh-Nagumo model, a two-time-scale model similarly organized by a single scalar *hysteresis* nonlinearity.

With enough time-scale separation, the (temporal) patterns exhibited by the trajectories of those models are robust and modulable in the parameter space, because they are in one-to-one correspondence with the persistent bifurcation diagrams of the universal unfolding of the hysteresis and winged-cusp, respectively.

We showed that this feature is of prime interest in neurophysiology, for instance, because it provides insight in the physiological parameters that can regulate the continuous transition between distinct temporal patterns as observed in experimental neuronal recordings.

The present paper pursues this investigation by adding diffusion in the three-scale temporal model and exploring the resulting three-scale spatio-temporal patterns: traveling bursts and standing bursts.

The close relationship of the model with its two-dimensional counterpart is of great help in the analysis because we extensively rely on the existing theory for two-scale models with a hysteresis nonlinearity. We study the existence of traveling bursts and standing bursts in our three-scale model by mimicking the analysis of traveling pulses and standing pulses in earlier two-scale models. This geometric analysis exploits the singular limit to construct the skeleton of the attractor and relies on Fenichel theory to show the persistence of the pattern away from the singular limit.

The results that we present are in close analogy both with the temporal results of the three-dimensional model [1] and with the spatiotemporal results in two-scale models [2, 3, 4, 5, 6]. We prove existence results when they follow from the existing Fenichel theory and discuss sensible predictions in situations that require an extension of the existing geometric theory. The conceptual message of the paper is that singularity theory provides a principled methodology for a geometric study of spatiotemporal patterns that can be robustly modulated in the presence of two or more well separated temporal and/or spatial scales.

Multi-scale patterns seem particularly relevant in biology. Traveling bursts play a major role in neuronal dynamics, both during development [7] and in the adult [8]. Morphogenetic fields with multiple characteristic spatial scales are hypothesized, for instance, in limb development [9]. More generally, we suggest that singularity theory provides a novel perspective to model phenomena involving multi-scale communication via traveling waves and multi-scale pattern formation.

Mathematically, three components reaction diffusion equations were studied in [10] but the organizing singularity was the hysteresis and the objects under analysis were single pulses, eventually interacting, rather geometric bursts. Traveling bursts were also observed in a biophysical neuronal network model in [11, Fig. 12.3]. Averaging over the fast time-scale was used to reduce existence and stability analysis to the classical traveling pulse analysis.

The paper is organized as follows. We introduce the three-scale reaction-diffusion model under analysis in Section 2. The system equations are prepared to be studied geometrically in Section 3, where we also recall some classical geometric tools for the analysis of traveling and standing pulses. Our presentation heavily relies on the ideas in [5, 6]. We develop the fine (fast/short-range), medium (slow/long-range), and gross (ultraslow/ultra-long-range) scale analysis in Sections 4, 5, and 6, respectively. Section 4 revisits the existence of traveling and standing fronts around the winged-cusp nonlinearity. Section 5 proves the co-existence of a homogenous resting state with a periodic wave-train or an infinite periodic pattern. Finally, the existence of traveling bursts is proved in Section 6.1

and the existence of standing bursts is conjectured (together with a detailed singular construction) in Section 6.2. Based on this geometric analysis, and in full analogy with [1], Section 7 discusses the relevance of the proposed model to study the modulation of spatio-temporal bursting. Open questions raised by the results of this paper are discussed theoretically and numerically in Section 8.

2 A three-scale reaction diffusion model

The paper studies spatio-temporal bursting in the reaction diffusion model

$$\tau_u u_t = D_u u_{xx} + g_{\text{wcusp}}(u, \lambda + w, \alpha + z, \beta, \gamma), \quad (1a)$$

$$\tau_w w_t = D_w w_{xx} + u - w. \quad (1b)$$

$$\tau_z z_t = D_z z_{xx} + u - z \quad (1c)$$

where $\tau_u, \tau_w, \tau_z > 0$, $D_u > 0$, and $D_w, D_z \geq 0$. The function

$$g_{\text{wcusp}}(u, \lambda, \alpha, \beta, \gamma) = -u^3 - \lambda^2 - \alpha + \beta u + \gamma u \lambda$$

is a universal unfolding of the winged cusp $-u^3 - \lambda^2$. We regard (1) as a one-component reaction-diffusion model organized by the winged-cusp singularity and with (spatio-temporal) adaptation variables w and z .

The fundamental hypothesis of model (1) is a hierarchy of scales between the “master” variable u and the adaptation variables w and z . This hierarchy of scales is consistent with the hierarchy between the state variable (u), the bifurcation parameter (λ), and unfolding parameters (α, β, γ) in singularity theory applied to bifurcation problems [12]. The variable w accounts for variations of the bifurcation parameter while the variable z accounts for variations of the unfolding parameter α . The fine-grain dynamics is organized by a single nonlinearity, with distinct behaviors depending on the bifurcation parameter and unfolding parameters. The medium-grain dynamics model (linear) adaptation of the bifurcation parameter to the quasi steady-state of the fine-grain behavior. The gross-grain dynamics models (linear) adaptation of unfolding parameters to the quasi steady-state behavior of the fine and medium grains.

We study separately the role of a time-scale separation

$$0 < \frac{\tau_u}{\tau_z} =: \varepsilon_{us} \ll \frac{\tau_u}{\tau_w} =: \varepsilon_s \ll 1, \quad (2)$$

which leads to *traveling* burst waves, and the role of space-scale separation

$$\sqrt{\frac{D_z}{D_u}} =: \delta_{ul}^{-1} \gg \sqrt{\frac{D_w}{D_u}} =: \delta_l^{-1} \gg 1, \quad (3)$$

which leads to *standing* burst waves.

The proposed model extends earlier work in two directions:

- in the absence of diffusion, model (1) reduces to the bursting model analyzed in [1]. The results in [1] underlie the importance of a persistent bifurcation diagram in the universal unfolding of the winged cusp, the *mirrored hysteresis* (class 2 of the persistent bifurcation diagram of the winged cusp listed in [12, page 208]), as a key nonlinearity for obtaining robust three-time-scale bursting as ultra-slow adaptation around a slow-fast phase portrait with coexistence of a stable fixed point and a stable limit cycle [13].
- when the winged cusp nonlinearity is replaced by an universal unfolding of the hysteresis singularity

$$g_{hy}(u, \lambda, \beta) = -x^3 + \lambda + \beta x,$$

then (1) reduces to a FitzHugh-Nagumo-type model, which is the fundamental two-scale model of excitability [14], exhibiting traveling pulses under a time-scale separation [2][3] and standing pulses under a space-scale separation [4][6].

3 Methodology

3.1 Reduction to singularly perturbed ODEs

Under time-scale separation (2) and for $D_w = D_z = 0$, we study the existence of a traveling wave $(u, w, z) \left(\frac{x}{\sqrt{D_u}} + c \frac{t}{\tau_w} \right)$ that satisfies the second order ODE system

$$u'' = cu' - g_{\text{wcusp}}(u, \lambda + w, \alpha + z, \beta, \gamma), \quad (4a)$$

$$w' = \frac{\varepsilon_s}{c}(-w + u), \quad (4b)$$

$$z' = \frac{\varepsilon_{us}}{c}(-z + u), \quad (4c)$$

$$c' = 0, \quad (4d)$$

where $' := \frac{d}{d\xi}$ and $\xi = \frac{x}{\sqrt{D_u}} + c \frac{t}{\tau_w}$. We briefly discuss the persistence of this behavior for $D_w, D_z > 0$ in Section 6.1.1.

Under space-scale separation (3), we study the existence of a standing wave $(u, w, z) \left(\frac{x}{\sqrt{D_u}} \right)$ that satisfies the second order ODE system

$$u'' = -g_{\text{wcusp}}(u, \lambda + w, \alpha + z, \beta, \gamma), \quad (5a)$$

$$\frac{1}{\delta_l^2} w'' = w - u, \quad (5b)$$

$$\frac{1}{\delta_{ul}^2} z'' = z' + z - u, \quad (5c)$$

where $' = \frac{d}{dx}$.

Both in models (4) and (5), we will construct singular orbits exploiting the time-scale separation of the dynamics and rely on the persistence of those geometric objects away from the singular limit to prove existence of the bursting waves.

To apply geometric singular perturbation methods [15][16] to the analysis of (4) and (5) we trans-

form them to first order ODE systems. For (4) this transformation reads

$$u' = v_u, \tag{6a}$$

$$v'_u = cv_u - g_{\text{wcusp}}(u, \lambda + w, \alpha + z, \beta, \gamma), \tag{6b}$$

$$w' = \frac{\varepsilon_s}{c}(u - w), \tag{6c}$$

$$z' = \frac{\varepsilon_{us}}{c}(u - z), \tag{6d}$$

$$c' = 0. \tag{6e}$$

For (5) this transformation reads

$$u' = v_u, \tag{7a}$$

$$v'_u = -g_{\text{wcusp}}(u, \lambda + w, \alpha + z, \beta, \gamma), \tag{7b}$$

$$w' = \delta_l v_w, \tag{7c}$$

$$v'_w = \delta_l (w - u), \tag{7d}$$

$$z' = \delta_{ul} v_z, \tag{7e}$$

$$v'_z = \delta_{ul} (z - u). \tag{7f}$$

which makes the three-scale nature of (1) explicit under assumption (3).

3.2 The geometry of traveling and standing pulses

For future reference, we briefly recall here the geometric construction of traveling and standing pulses in two-scale reaction diffusion equations. Our exposition is based on [5, Sections 4 and 5] and [6, Section 4].

Let $g_{\text{hy}}(u, \lambda, \beta) = -u^3 + \beta u + \lambda$ be a universal unfolding of the hysteresis singularity. The two-scale reaction diffusion model

$$\tau_u u_t = D_u u_{xx} + g_{\text{hy}}(u, \lambda + w, \beta), \tag{8a}$$

$$\tau_w w_t = D_w w_{xx} + u - w, \tag{8b}$$

exhibits traveling pulses under time-scale separation (2) and standing pulses under space-scale separa-

tion (3). The traveling pulse is constructed geometrically for $D_w = 0$ using the traveling wave ansatz. The standing pulse is constructed geometrically in the standing wave ansatz. For large time-scale separation and large space-scale separation the two reductions lead to the singularly perturbed ordinary differential equations

$$u' = v_u, \quad (9a) \qquad u' = v_u, \quad (10a)$$

$$v'_u = cv_u - g_{\text{hy}}(u, \lambda + w, \beta), \quad (9b) \qquad v'_u = -g_{\text{hy}}(u, \lambda + w, \beta), \quad (10b)$$

$$w' = \frac{\varepsilon_s}{c}(u - w), \quad (9c) \qquad w' = \delta_l v_w, \quad (10c)$$

$$c' = 0, \quad (9d) \qquad v'_w = \delta_l(w - u). \quad (10d)$$

(traveling)

(standing)

The singular skeleton of (9) and (10) is sketched in Figure 1. Both the traveling and standing pulses are homoclinic orbits obtained as perturbations of singular homoclinic orbits.

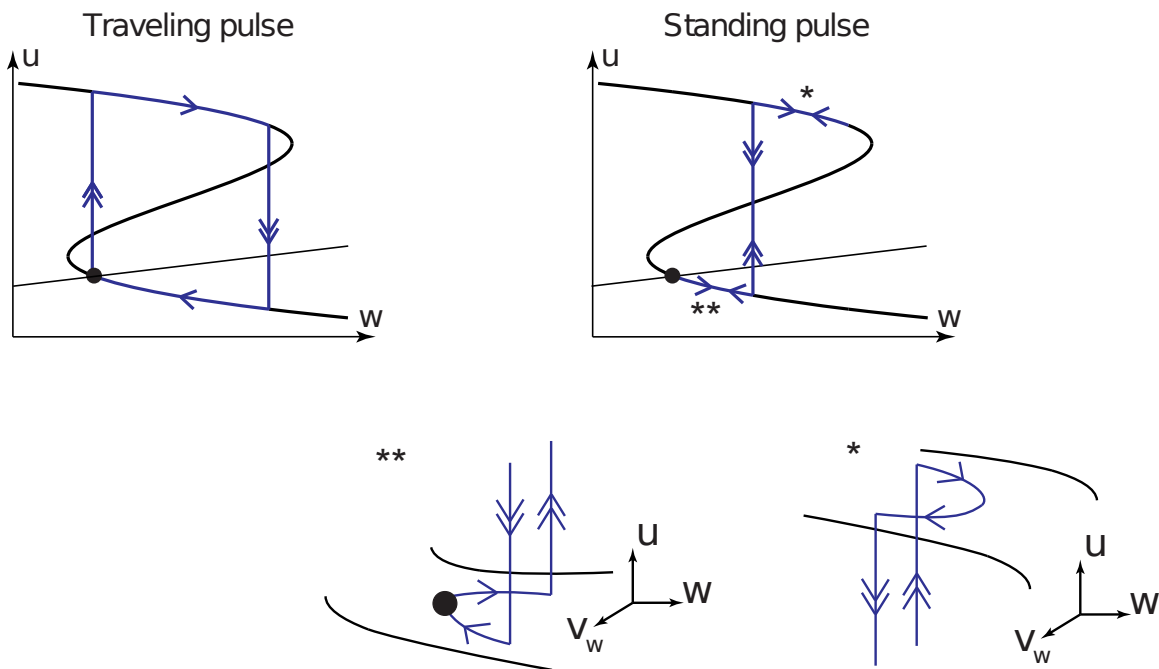


Figure 1: Geometry of traveling and standing pulses in reaction-diffusion model with a cubic nonlinearity.

The singular homoclinic orbit associated to the *traveling* pulse is characterized by a first jump from steady-state to the excited state associated to the rising part of the pulse. This jump is a heteroclinic orbit of the fast-subsystem (9a-9b) corresponding to a front between homogeneous steady-states of (8a) traveling with speed $c^* \neq 0$. The value of c^* is determined by imposing the transverse intersection

of suitable unstable and stable manifolds of the fast dynamics. On the upper branch of the critical manifold, the trajectory slides according to the reduced (slow) dynamics associated to (9) until it reaches a second downward fast heteroclinic jump and then slowly converges back to rest.

Due to the Hamiltonian nature of (10), the *standing* pulse is a symmetric homoclinic orbit, that is, satisfying $(u(\xi), v_u(\xi), w(\xi), v_w(\xi)) = (u(-\xi), -v_u(-\xi), w(-\xi), -v_w(-\xi))$. It therefore suffices to construct a singular trajectory originating at the steady state and intersecting transversely the subspace $\{v_u = v_w = 0\}$. Continuation of this trajectory provides the full singular symmetric homoclinic orbit. The first portion of this trajectory is “slow” and it is given by the (one-dimensional) unstable manifold of the steady state inside the (two-dimensional) critical manifold of (10), that is, with respect to its reduced dynamics. When it reaches the heteroclinic jump, the trajectory jumps to the excited states. On the upper branch of the critical manifold, the trajectory is carried transversely across $\{v_u = v_w = 0\}$ by the reduced flow. The other half of the trajectory is constructed by symmetry.

4 Fine-scale analysis: bistability and connecting fronts

For $\varepsilon_s = \varepsilon_{us} = 0$ and $\delta_l = \delta_{ul} = 0$, models (6) and (7) reduce to one-scale behaviors describing the fine-grain dynamics:

$$u' = v_u, \quad (11a) \qquad u' = v_u, \quad (12a)$$

$$v'_u = cv_u - g_{\text{wcusp}}(u, \tilde{\lambda}, \tilde{\alpha}, \beta, \gamma), \quad (11b) \qquad v'_u = -g_{\text{wcusp}}(u, \tilde{\lambda}, \tilde{\alpha}, \beta, \gamma), \quad (12b)$$

(traveling)

(standing)

where $\tilde{\lambda}$, $\tilde{\alpha}$, c , w , and z are now fixed parameters.

In both models, the steady-state

$$\{(u, v_u) : v = 0, g_{\text{wcusp}}(u, \tilde{\lambda}, \tilde{\alpha}, \beta, \gamma) = 0\} \quad (13)$$

is determined by the universal unfolding of the winged cusp, as the bifurcation and unfolding parameters vary. For $\gamma = 0$, $\beta > 0$, and $\tilde{\alpha} = -2\left(\frac{\beta}{3}\right)^{2/3}$, the steady-state curve possesses a transcritical singularity for $\tilde{\lambda} = 0$, where two mirror-symmetric hysteretic branches merge, as sketched in Figure 2-A.

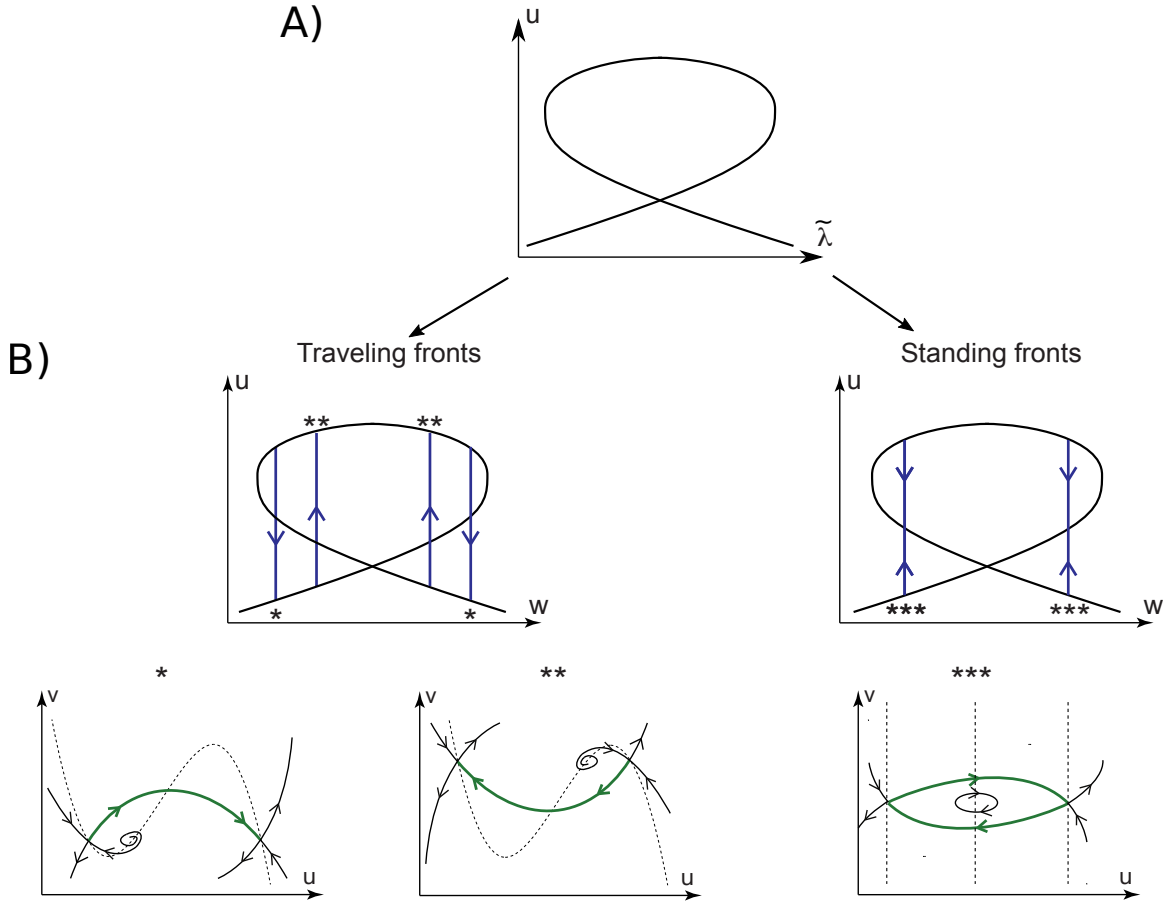


Figure 2: The geometry of traveling and standing wave fronts around a transcritical singularity.

Away from the transcritical singularity, both hysteretic branches possess the same qualitative geometry as the classical cubic critical manifold in Figure 1. In particular, they exhibit bistability between up and down homogeneous steady-states of the associated scalar reaction diffusion equation. Both in the traveling and standing case, there exist connecting heteroclinic orbits between the up and down steady-state branches (Figure 2-B), which correspond to traveling or standing wave fronts of the associated reaction diffusion equation. In the traveling case, there are four c -dependent values of the bifurcation parameter $\tilde{\lambda}$ for which the model possesses a heteroclinic orbit: two upward heteroclinic orbits and two downward heteroclinic orbits. In the standing case, there are two values of the bifurcation parameter $\tilde{\lambda}$ for which the model possesses both a downward and an upward heteroclinic orbit. The phase-portraits of the fast heteroclinic jumps are sketched in the insets.

Existence of these heteroclinic orbits follows exactly from the theory in [5, Section 4.5] for the traveling case and in [6, Section 4] for the standing case. They all persist to parameter variations, in particular, to unfolding of the transcritical singularity. We omit here a detailed proof but the key derivations are recalled in Lemma A.1 for the traveling case and in Lemma B.1 for the standing case.

5 Medium-scale analysis: bistability between homogeneous and periodic states

To model slow adaptation of the bifurcation parameter λ , we unfreeze the slow variable w and study coexistence of a resting state and a limit cycle in the models

$$u' = v_u, \quad (14a) \qquad u' = v_u, \quad (15a)$$

$$v'_u = cv_u - g_{\text{wcusp}}(u, \lambda + w, \tilde{\alpha}, \beta, \gamma), \quad (14b) \qquad v'_u = -g_{\text{wcusp}}(u, \lambda + w, \tilde{\alpha}, \beta, \gamma), \quad (15b)$$

$$w' = \frac{\varepsilon_s}{c}(u - w), \quad (14c) \qquad w' = \delta_l v_w, \quad (15c)$$

$$c' = 0, \quad (14d) \qquad v'_w = \delta_l(w - u), \quad (15d)$$

(traveling)

(standing)

for ε_s and δ_l sufficiently small, respectively. This bistability is the generalization of bistability between the homogeneous rest and excited states in the two-scale scenario.

For future reference, we make the following preliminary observation. The homogeneous resting state equation of (14) and (15) is

$$F(u, \lambda, \tilde{\alpha}, \beta, \gamma) := -u^3 - (\lambda + u)^2 + \beta u - \gamma(\lambda + u)u - \tilde{\alpha} = 0 \quad (16)$$

and is easily shown to be again a universal unfolding of the winged cusp around $u_{\text{wcusp}} := \frac{1}{3}$, $\lambda_{\text{wcusp}} := 0$, $\alpha_{\text{wcusp}} := -\frac{1}{27}$, $\beta_{\text{wcusp}} := -\frac{1}{3}$, $\gamma_{\text{wcusp}} := -2$.

5.1 Traveling case

The two-dimensional critical manifold of the singularly perturbed dynamics (14) is

$$\{(u, v_u, w, c) : v_u = 0, g_{\text{wcusp}}(u, \lambda + w, \tilde{\alpha}, \beta, \gamma) = 0\} \quad (17)$$

For $\gamma = 0$, $\beta > 0$, and $\tilde{\alpha} < -2\left(\frac{\beta}{3}\right)^{2/3}$ the transcritical singularity in Figure 2-A unfolds into the mirrored hysteresis persistent bifurcation diagram introduced in [1, Section 2.3] and organizing the singular phase portrait in Figure 3-A. This algebraic curve is a template for rest-spike bistability in

ordinary differential equations [13, Theorem 2]. Here we show that it is also a template to construct a wavefront between homogeneous resting and periodic wave-train.

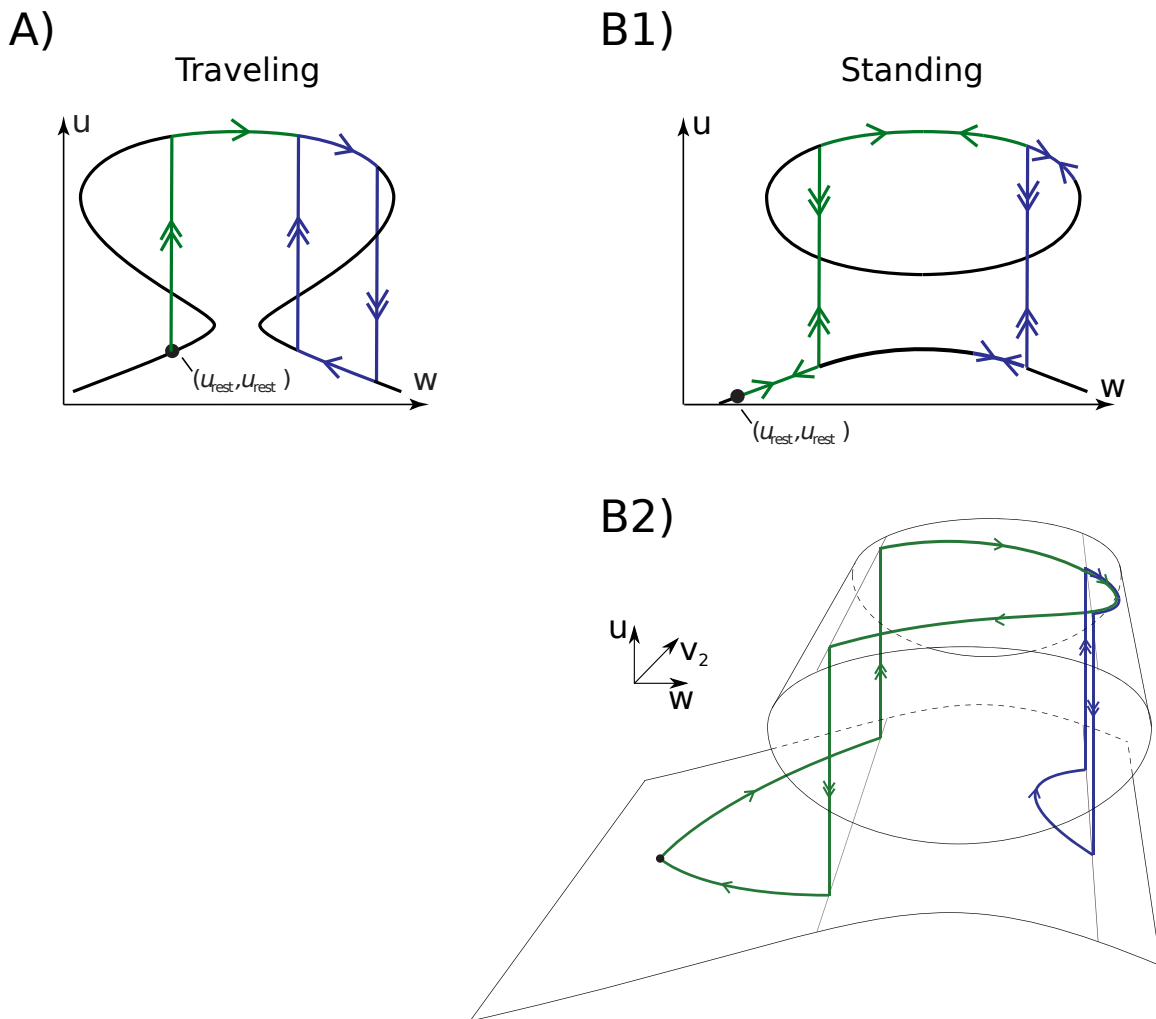


Figure 3: **A.** Bistability between a homogeneous steady state and a periodic wave-train in the singular limit and in the traveling wave ansatz. The two objects are connected by a heteroclinic orbit. **B.** Bistability between a homogeneous steady state and an infinite periodic pattern in the singular limit and in the standing wave ansatz. There exists a homoclinic orbit to the homogeneous steady-state that shadows the infinite periodic pattern.

The singular phase portrait of (14) in Fig 3-A exists for a precise value of $c = c^*$ derived in Lemma A.1 by imposing the intersection of suitable stable and unstable manifolds. It contains an equilibrium (black dot) corresponding to a stable homogeneous resting state of the associated reaction diffusion model, a singular periodic solution (blue line) corresponding to a traveling periodic wave train, and a heteroclinic¹ orbit (green line) corresponding to a traveling wave front connecting the stable homogeneous resting state to the periodic wave train. The periodic solution consists of two heteroclinic jumps of the layer dynamics (18) connected by trajectories of the reduced dynamics (19):

¹The term heteroclinic is used in the generalized sense of a trajectory connecting two ω -limit sets, not necessarily two fixed points.

$$u' = v_u, \quad (18a) \quad 0 = v_u, \quad (19a)$$

$$v'_u = cv_u - g_{\text{wcusp}}(u, \lambda + w, \tilde{\alpha}, \beta, \gamma), \quad (18b) \quad 0 = cv_u - g_{\text{wcusp}}(u, \lambda + w, \tilde{\alpha}, \beta, \gamma), \quad (19b)$$

$$w' = 0, \quad (18c) \quad w' = \frac{1}{c}(u - w), \quad (19c)$$

$$c' = 0 \quad (18d) \quad c' = 0, \quad (19d)$$

The heteroclinic orbit consists of a heteroclinic jump of the layer dynamics followed by a trajectory of the reduced dynamics. The fast phase portrait associated to upward (resp. downward) heteroclinic jumps is exactly the same as in Figure 2-B* (resp. Figure 2-B**). This singular structure persists for $\varepsilon_s > 0$, as proved in the following theorem.

Theorem 1 *There exist open sets of bifurcation (λ) and unfolding (α, β, γ) parameters in a parametric neighborhood of the pitchfork singularity of (16) at $\beta = \frac{1}{3}$, $\lambda = \frac{1}{3}$, $\tilde{\alpha} = \frac{1}{27} - \frac{1}{9}$, $\gamma = 0$ such that, for all parameters in those sets, there exists $c^* \neq 0$ and $\bar{\varepsilon}_s > 0$ such that, for each $0 < \varepsilon_s < \bar{\varepsilon}_s$, model (14) possesses for a value $\bar{c} = c^* + \mathcal{O}(\varepsilon)$ a fixed point and a limit cycle both of saddle type and a heteroclinic orbit h_ε converging in backward time to the fixed point and in forward time to the limit cycle.*

Theorem 1 generalizes bistability between a fixed point and a limit cycle in finite dimensional systems [1, Theorem 2] to bistability between a homogeneous resting state and a periodic wave-train in reaction-diffusion models organized by the winged cusp singularity. We note that the heteroclinic orbit of Theorem 1 selects one out an infinity of periodic solutions for (14) by selecting a unique traveling speed.

5.2 Standing case

The two-dimensional critical manifold of the singularly perturbed dynamics (15) is

$$\{(u, v_u, w, v_w, c) : v_u = v_w = 0, g_{\text{wcusp}}(u, \lambda + w, \tilde{\alpha}, \beta, \gamma) = 0\} \quad (20)$$

For $\gamma = 0$, $\beta > 0$, $\tilde{\alpha} > -2\left(\frac{\beta}{3}\right)^{2/3}$, and $\left|\tilde{\alpha} + 2\left(\frac{\beta}{3}\right)^{2/3}\right|$ sufficiently small, the transcritical singularity in Figure 2-A unfolds into the persistent bifurcation diagram organizing the singular phase portrait in Figure 3-B1. This persistent bifurcation diagram is qualitatively different from the mirrored hysteresis

in Figure 3-A but both diagrams belong to the unfolding of the same transcritical singularity in the universal unfolding of the winged cusp.

The singular phase portrait in Figure 3-B contains an equilibrium (black dot) corresponding to a stable homogeneous resting state of the associated reaction diffusion model, a singular periodic solution (blue line) corresponding to a periodic pattern, and a singular homoclinic orbit (green line) corresponding to a standing pulse. The singular periodic and the homoclinic solution share a common arc. The 3D projection of this singular phase-portrait onto the (u, w, v_2) space is sketched in Figure 3-B2. Both the periodic and homoclinic solutions consist of two heteroclinic jumps of the layer dynamics (21) connected by trajectories of the reduced dynamics (22):

$$u' = v_u, \quad (21a) \quad 0 = v_u, \quad (22a)$$

$$v'_u = -g_{\text{wcusp}}(u, \lambda + w, \tilde{\alpha}, \beta, \gamma), \quad (21b) \quad 0 = -g_{\text{wcusp}}(u, \lambda + w, \tilde{\alpha}, \beta, \gamma), \quad (22b)$$

$$w' = 0, \quad (21c) \quad w' = v_w, \quad (22c)$$

$$v'_w = 0, \quad (21d) \quad v'_w = u - w. \quad (22d)$$

The fast phase portrait associated to the heteroclinic jumps is exactly the same as in Figure 2 (case***). This singular structure persists for $\delta_l > 0$.

Theorem 2 *There exist open sets of bifurcation (λ) and unfolding $(\tilde{\alpha}, \beta, \gamma)$ parameters in a parametric neighborhood of the pitchfork singularity of (16) at $\beta = \frac{1}{3}$, $\lambda = \frac{1}{3}$, $\tilde{\alpha} = \frac{1}{27} - \frac{1}{9}$, $\gamma = 0$ such that, for all parameters in those sets, there exists $\bar{\delta}_l > 0$ such that, for all $0 < \delta_l < \bar{\delta}_l$, model (15) possesses a homoclinic trajectory and a limit cycle that are $\mathcal{O}(\delta_l)$ -close to each other together with their unstable manifolds in a neighborhood of the point $(u_{max}, 0, w_{max}, 0)$ where w reaches its (unique) maximum along the singular homoclinic trajectory.*

Theorem 2 characterizes bistability between a homogeneous resting state and a periodic pattern in reaction diffusion models organized by the winged cusp singularity. We note that the homoclinic orbit singles out a privileged periodic pattern in model (15) out of an infinity of them.

6 Gross scale analysis: traveling and standing bursts

6.1 Traveling bursts

Very much like traveling pulses are homoclinic orbits of the singularly perturbed dynamics (9), traveling bursts are constructed as homoclinic orbits of the singularly perturbed dynamics (6). We start from the singular limit of this homoclinic orbit, which consists of heteroclinic jumps obeying the layer dynamics (23) connected by trajectories of the reduced dynamics (24):

$$u' = v, \quad (23a) \quad 0 = v, \quad (24a)$$

$$v' = cv - g_{\text{wcusp}}(u, \lambda + w, \alpha + z, \beta, \gamma), \quad (23b) \quad 0 = cv - g_{\text{wcusp}}(u, \lambda + w, \alpha + z, \beta, \gamma), \quad (24b)$$

$$w' = 0, \quad (23c) \quad w' = \frac{1}{c}(u - w), \quad (24c)$$

$$z' = 0, \quad (23d) \quad z' = \frac{\varepsilon_{us}}{c\varepsilon_s}(u + \bar{z} - z), \quad (24d)$$

$$c' = 0, \quad (23e) \quad c' = 0. \quad (24e)$$

The overall geometry of the singular homoclinic orbit is illustrated in Figure 4.

Figure 4-A illustrates the deformation of the singular phase portrait of the medium scale dynamics (14) for different values of the unfolding parameter $\tilde{\alpha}$. The starting point (at z_{rest}) is determined by Theorem 1, which corresponds to the phase portrait in Figure 3A. This situation is created by picking $(\lambda, \tilde{\alpha}, \beta, \gamma)$ and $c = c^*$ as in Theorem 1, and $\alpha = \tilde{\alpha} - u_{rest}$ so that $(u_{rest}, u_{rest}, u_{rest})$ is an equilibrium. Lemma C.1 shows that, for $z > z_{rest}$, the fixed point and the limit cycle persist over a range $[z_{rest}, z^*)$, but that the fast heteroclinic orbit from the lower to the upper branch of the critical manifold progressively slides toward the second upward heteroclinic orbit as $z \rightarrow z^*$. For $z > z^*$ only the fixed point and the downward heteroclinic orbit persist.

The singular homoclinic orbit is constructed by spanning the range $[z_{rest}, z^* + \theta]$, for small $\theta > 0$, as illustrated in Figure 4B. As for the traveling pulse, a first heteroclinic jump brings the orbit from rest to the excited state. As z increases in the “ultraslow” scale, the trajectory jumps between the lower and the upper branches of the critical manifold, shadowing the family of singular limit cycles, until $z > z^*$. The orbit then relaxes back to rest along the lower branch of the critical manifold.

The following theorem proves the existence of a homoclinic orbit that tracks the singular homoclinic orbit away from the singular limit. Its proof is a direct application of the Exchange Lemma, more

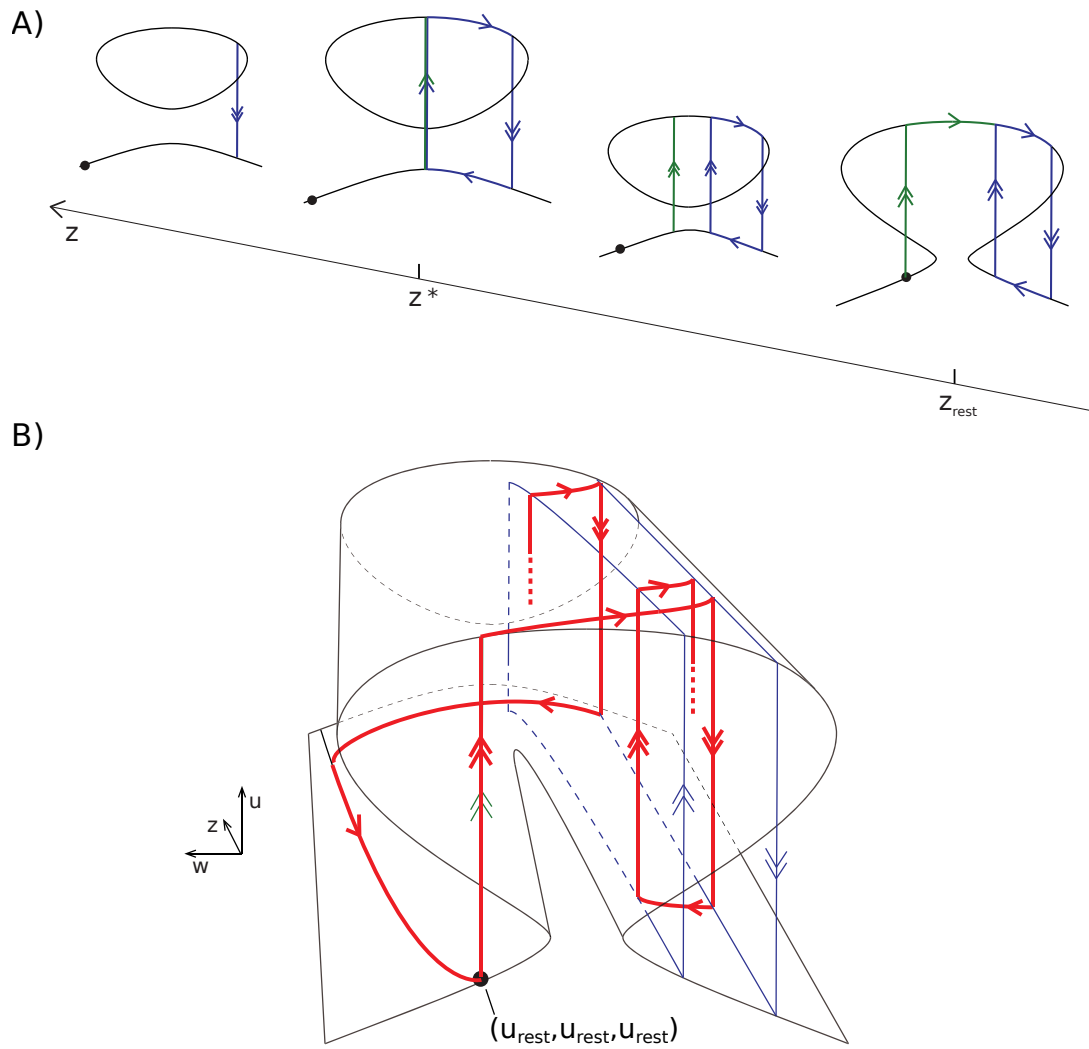


Figure 4: Geometric construction of traveling bursts.

precisely, of the theorem in [16, Section 4].

Theorem 3 *There exist open sets of bifurcation (λ) and unfolding (α, β, γ) parameters in a parametric neighborhood of the pitchfork singularity of (16) at $\beta = \frac{1}{3}$, $\lambda = \frac{1}{3}$, $\tilde{\alpha} = \frac{1}{27} - \frac{1}{9}$, $\gamma = 0$ such that, for almost all parameters in those sets, there exists $c^* \neq 0$ and $\bar{\varepsilon}_s > 0$ such that, for all $0 < \varepsilon_s < \bar{\varepsilon}_s$, there exists $\bar{\varepsilon}_{us} > 0$ such that, for all $0 < \varepsilon_{us} < \bar{\varepsilon}_{us}$, there exists $\bar{c} \neq 0$, such that model (6) possesses for a value $\bar{c} = c^* + \mathcal{O}(\varepsilon)$ a homoclinic orbit obtained as a $\mathcal{O}(\varepsilon_s)$ -perturbation of the singular traveling burst solution in Figure 4.*

6.1.1 Persistence of traveling bursts for non-zero D_w, D_z

For finite δ_l and δ_{ul} the transformation of (1) into a system of first order ODEs in the traveling wave ansatz reads

$$u' = v_u, \tag{25a}$$

$$v'_u = cv_u - g_{\text{wcusp}}(u, \lambda + w, \alpha + z, \beta, \gamma), \tag{25b}$$

$$w' = v_w, \tag{25c}$$

$$v'_w = c \frac{\delta_l^2}{\varepsilon_s} v_w + \delta_l^2 (w - u), \tag{25d}$$

$$z' = v_z, \tag{25e}$$

$$v'_z = c \frac{\delta_{ul}^2}{\varepsilon_{us}} v_z + \delta_{ul}^2 (z - u), \tag{25f}$$

$$c' = 0, \tag{25g}$$

Both linear subsystems (25c-25d) and (25e-25f) are themselves slow-fast systems. Dropping the subscripts, they both have an eigenvalue which is $\mathcal{O}\left(\frac{\varepsilon}{c\delta^2}\right)$ and another eigenvalue which is $\mathcal{O}\left(\frac{c\delta^2}{\varepsilon}\right)$. For finite c and δ , the two eigenvalues are sharply separated, provided that

$$\frac{\varepsilon_s}{c\delta_l^2} \ll 1, \quad \frac{\varepsilon_{us}}{c\delta_{ul}^2} \ll 1 \tag{26}$$

which, for finite c , is always satisfied for sufficiently large time-scale separation. In the singular limit (26), we can project both (25c-25d) and (25e-25f) on their respective slow manifolds $c \frac{\delta_l^2}{\varepsilon_s} v_w + \delta_l^2 (w - u) = 0$ and $c \frac{\delta_{ul}^2}{\varepsilon_{us}} v_z + \delta_{ul}^2 (z - u) = 0$. Performing this projection reduces (25) to (6). Note that (26) is automatically verified if $D_w = D_z = 0$ because in this case $\delta_l = \delta_{ul} = +\infty$. For finite $\delta_l = \delta_{ul}$, the

singular limit (26) introduces two extra time-scales corresponding to the $\mathcal{O}(1/\varepsilon_{s,us})$ eigenvalues. The presence of more than two time-scales impedes a straightforward application of the Exchange Lemma. We do not develop this singular limit in more details here.

6.2 Standing bursts

In analogy with the standing pulses of (10), the standing bursts of the singularly perturbed dynamics (7) are symmetric homoclinic orbits, that is, they satisfy

$$(u(\xi), v_u(\xi), w(\xi), v_w(\xi), z(\xi), v_z(\xi)) = (u(-\xi), -v_u(-\xi), w(-\xi), -v_w(-\xi), z(-\xi), -v_z(-\xi)).$$

The overall geometry of the associated symmetric *singular* homoclinic orbit is illustrated in Figure 5.

Figure 5A illustrates the deformation of the singular phase portrait of the medium scale dynamics (15) for different values of the unfolding parameter $\tilde{\alpha}$. The existence of the range (z_{hom}, \bar{z}_{hom}) follows from Theorem 2, which corresponds to the phase portrait in Figure 3B. The condition $z_{rest} \in (z_{hom}, \bar{z}_{hom})$ is again imposed by picking $(\lambda, \tilde{\alpha}, \beta, \gamma)$ as in Theorem 2, and $\alpha = \tilde{\alpha} - u_{rest}$. Lemma B.1 also shows the existence of $z^* > \bar{z}_{hom}$ such that, for $z > z^*$, no fast heteroclinic orbits persist.

The singular symmetric homoclinic orbit is constructed by first considering the singular limit in which (u, v_u, w, v_w) are fast and (z, v_z) are slow. The associated layer and reduced dynamics are

$$u' = v_u, \quad (27a) \quad 0 = v_u, \quad (28a)$$

$$v'_u = -g_{w\text{cusp}}(u, \lambda + w, \alpha + z, \beta, \gamma), \quad (27b) \quad 0 = -g_{w\text{cusp}}(u, \lambda + w, \alpha + z, \beta, \gamma), \quad (28b)$$

$$w' = \varepsilon_w v_w, \quad (27c) \quad 0 = v_w, \quad (28c)$$

$$v'_w = \varepsilon_w (w - u), \quad (27d) \quad 0 = (w - u), \quad (28d)$$

$$z' = 0, \quad (27e) \quad z' = v_z, \quad (28e)$$

$$v'_z = 0, \quad (27f) \quad v'_z = z - u - \bar{z}. \quad (28f)$$

In this singular limit, as in the case of the standing pulse, the homogeneous resting state belongs to a 2-dimensional critical manifold and, inside this manifold (*i.e.*, with respect to the reduced dynamics (28)), it has one dimensional stable and unstable manifolds (Figure 5B). The unstable manifold pro-

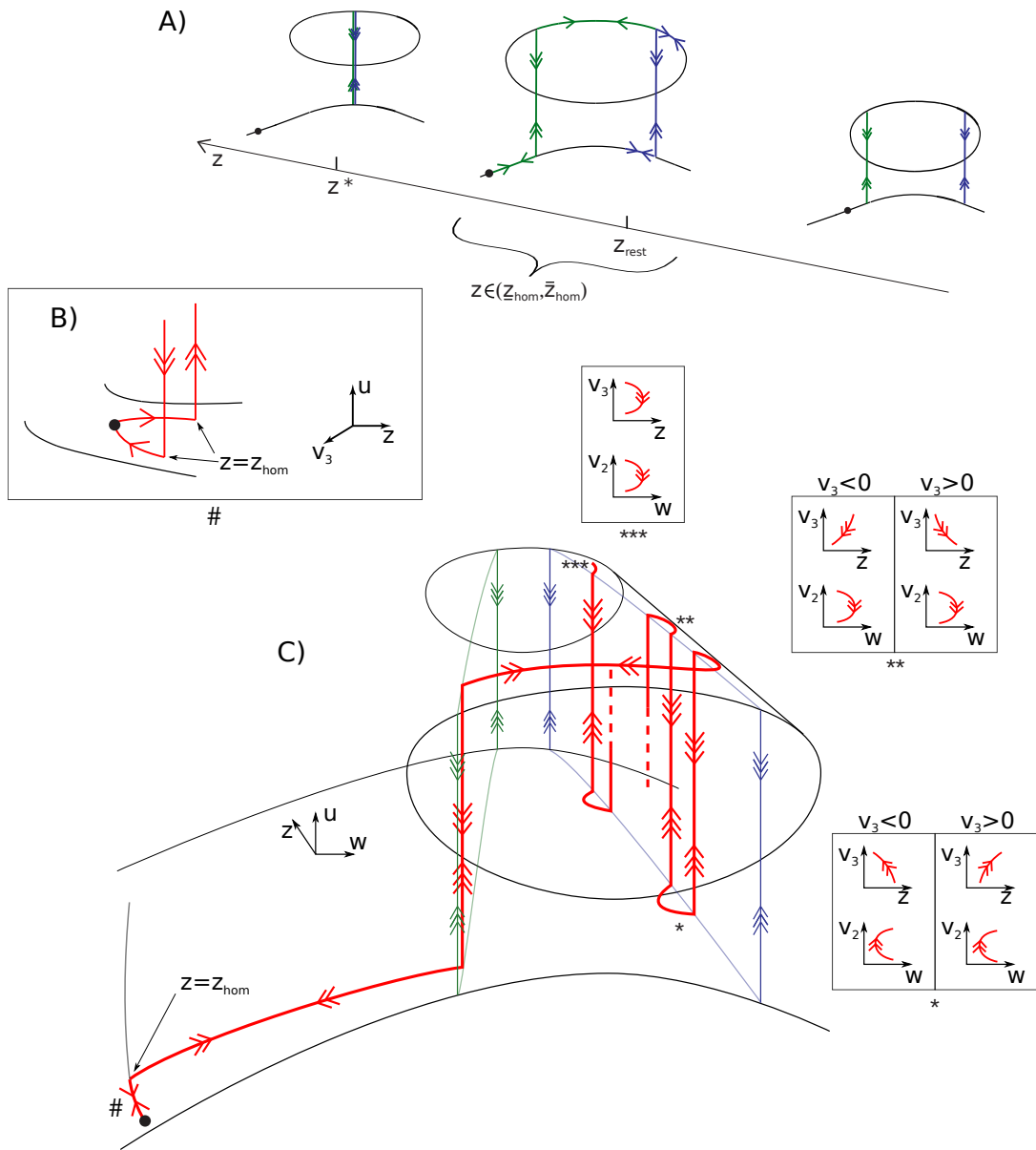


Figure 5: Geometric construction of standing bursts. In **B.** and **C.**, one arrow distinguishes trajectories of the reduced dynamics (28), two arrows trajectories of the reduced dynamics (30), and three arrows trajectories of the layer dynamics (29).

vides the first portion of the singular homoclinic orbit. Note that both u and w are at quasi steady state in this regime.

The reduced and layer dynamics (27) and (28) are not appropriate to describe the oscillatory part of the pattern because only (u, v_u) are at their quasi steady-state (except during jumps). In this new singular limit, (w, v_w) are part of the slow subsystem, that is, the layer and reduced dynamics are

$$u' = v_u, \quad (29a) \quad 0 = v_u, \quad (30a)$$

$$v'_u = -g_{\text{wcusp}}(u, \lambda + w, \alpha + z, \beta, \gamma), \quad (29b) \quad 0 = -g_{\text{wcusp}}(u, \lambda + w, \alpha + z, \beta, \gamma), \quad (30b)$$

$$w' = 0, \quad (29c) \quad w' = v_w, \quad (30c)$$

$$v'_w = 0, \quad (29d) \quad v'_w = w - u, \quad (30d)$$

$$z' = 0, \quad (29e) \quad z' = \frac{\delta_{ul}}{\delta l} v_z, \quad (30e)$$

$$v'_z = 0, \quad (29f) \quad v'_z = \frac{\delta_{ul}}{\delta l} (z - u - \bar{z}). \quad (30f)$$

The oscillatory part of the standing burst solution (Figure 5 C) is composed by trajectories of the reduced dynamics (30) connected by heteroclinic jumps of the layer dynamics (29). Projections of the slow orbits onto the (w, v_w, z, v_z) -space are drawn in the insets marked with stars. Each slow orbit crosses transversely the subspace $v_w = 0$. The last slow orbit crosses transversely the subspace $\{v_w = v_z = 0\}$, which makes the singular trajectory symmetric, in view of the fact that v_u is identically zero on the critical manifold.

The quasi-steady state part of the standing burst, ruled by (28), connects to the oscillatory part of the standing burst, ruled by (29), (30), at a value z_{hom} , where the singular trajectory leaves the quasi-steady branch. Let $W_{q.s.s}^u$ be the (three-dimensional) manifold obtained by the union of the (two-dimensional) unstable manifolds of the fixed points of the layer dynamics (27) lying on the quasi-steady state branch. Then z_{hom} can be found by tracking $W_{q.s.s}^u$ along (29), (30) and imposing its (zero-dimensional) transverse intersection with the (three-dimensional) $\{v_u = v_w = v_z = 0\}$ subspace, much in the same way as [6, Lemma 4.2].

The overall singular homoclinic orbit is constructed by patching two pieces corresponding to the two different singular limits. In contrast to traveling bursts, a proof of its persistence away from the singular limit(s) does not follow as an immediate application of the Exchange Lemma. However, due to transversality, its persistence is highly plausible, leading to the following conjecture.

Conjecture 1 *There exist open sets of bifurcation (λ) and unfolding (α, β, γ) parameters in a parametric neighborhood of the pitchfork singularity of (16) at $\beta = \frac{1}{3}$, $\lambda = \frac{1}{3}$, $\tilde{\alpha} = \frac{1}{27} - \frac{1}{9}$, $\gamma = 0$ such that, for almost all parameters in those sets, there exists $\bar{\delta}_l > 0$ such that, for all $0 < \delta_l < \bar{\delta}_l$, there exists $\bar{\delta}_{ul} > 0$ such that, for all $0 < \delta_{ul} < \bar{\delta}_{ul}$, model (7) possesses a homoclinic orbit obtained as a $\mathcal{O}(\delta_l)$ -perturbation of the singular standing burst solution in Figure 5.*

7 Modulation of spatio-temporal bursting

A main motivation in [1] to study a model organized by the winged cusp singularity is that it provides a principled way to analyze the continuous deformation of bursting patterns as parameter paths in the universal unfolding of the singularity. The same geometric picture generalizes to spatio-temporal behaviors.

By changing the value of the bifurcation parameter λ and of the unfolding parameter α the traveling burst pattern predicted by Theorem 3 continuously deforms to a classical traveling pulse (Figure 6). This is easily understood in terms of the geometry of the singular limit of the slow-fast subsystem. In particular, in the parameter region where there is no bistability in the slow-fast system, we recover the geometry of the Fitzugh-Nagump model, as the ultra-slow variable barely affects the traveling pulse.

The same result holds for continuous deformation of standing bursts into standing pulses. By changing the value of the bifurcation parameter λ and of the unfolding parameters α and β the standing burst pattern predicted by Conjecture 1 is changed into a classical standing pulse (Figure 7). Again, inspection of the geometry of the singular limit of the short-long range subsystem reveals the qualitative analogy with the geometry of the classical standing pulse solution and the presence of the ultra-long-range variable barely affects the standing pulse solution.

8 Discussion

8.1 Stability of bursting waves

Our work establishes the existence, not the stability, of traveling and standing bursting waves. The stability analysis is beyond the scope of the present paper but predictions can be made in accordance with what is known about the stability of the two-scale models with a cubic nonlinearity. Standing pulses in two-scale models are known to be stable if the space-scale separation δ_s is much smaller than

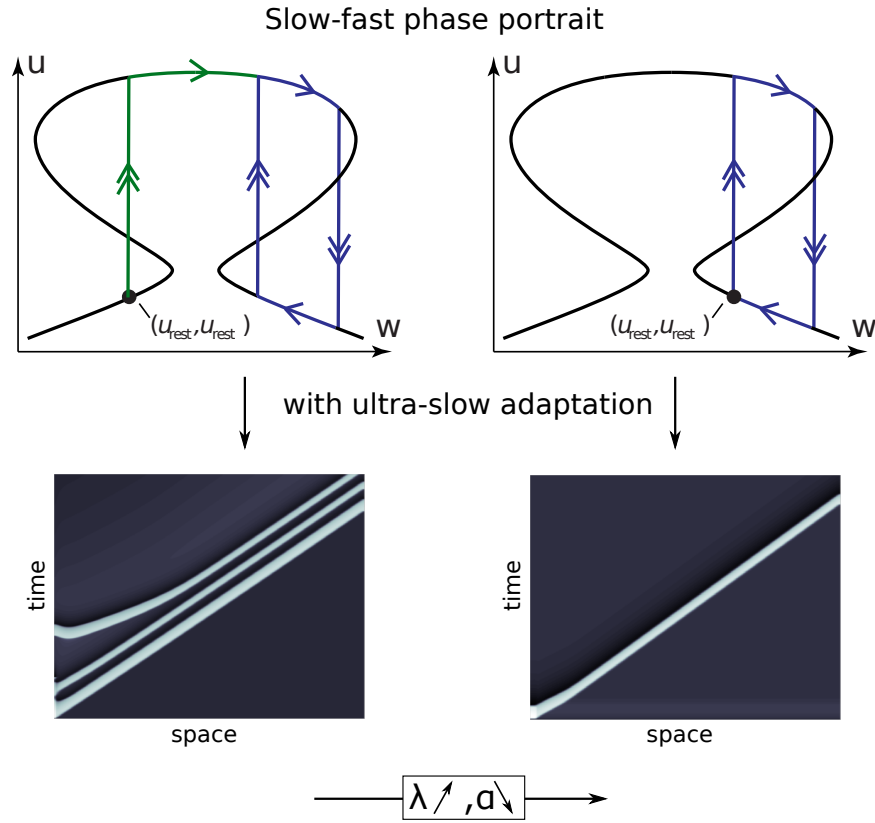


Figure 6: Parameters for traveling burst (left plot) are the same as Figure 8. Parameters for traveling pulse (right plot) are the same as traveling bursts except $\lambda = \lambda_{PF}(\beta) + 0.15$ and $\alpha = \alpha_{PF}(\beta) + 0.4$

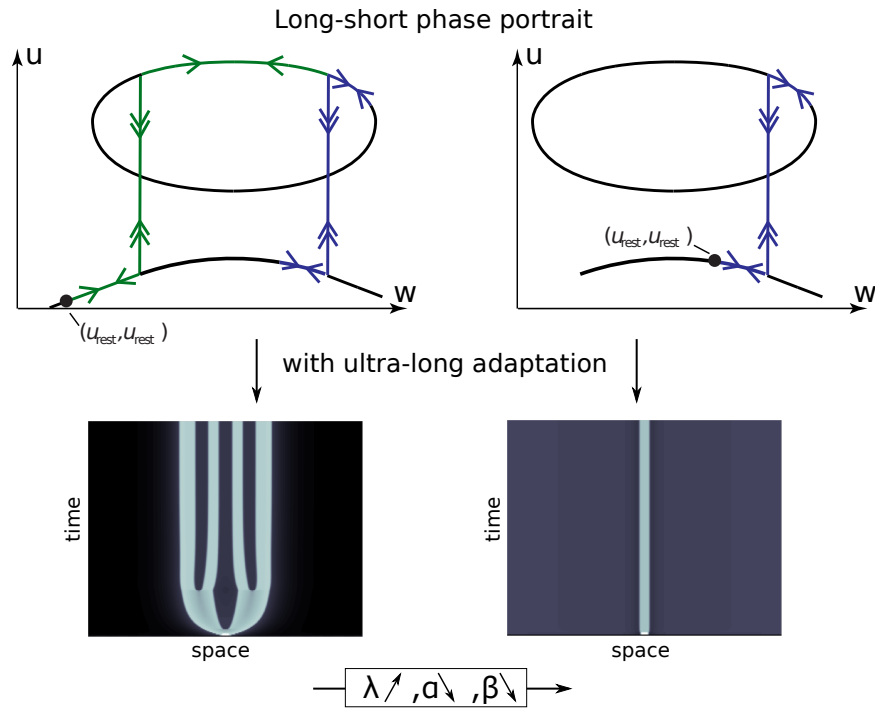


Figure 7: Parameters standing burst (left plot) are the same as Figure 10. Parameters for standing pulse are the same as standing bursts except $\lambda = \lambda_{PF}(\beta) + 0.1$, $\alpha = \alpha_{PF}(\beta) + 0.385$ and $\beta = 1/3$.

the time-scale separation [17, Theorem 4.2], namely

$$\delta_l \ll \varepsilon_s$$

Likewise, to the best of our knowledge, the stability of traveling pulses has been analyzed only in the absence of diffusion in the adaptation variable [3], which corresponds to the limit

$$\delta_l = \infty,$$

but one can expect that traveling pulses are stable when space-scale separation dominates the time-scale separation, i.e.

$$\varepsilon_s \ll \delta_l.$$

We suspect that similar properties extend to the three-scale model analyzed in the present paper : traveling burst should be stable when time-scale separation dominates space-scale separation, namely

$$\delta_l \ll \varepsilon_s, \text{ and } \delta_{ul} \ll \varepsilon_{us},$$

and standing bursts should be stable when space-scale separation dominates time-scale separation

$$\delta_l \gg \varepsilon_s, \text{ and } \delta_{ul} \gg \varepsilon_{us}.$$

8.1.1 Numerical illustration

The following numerical examples were obtained with MATLAB function `pdepe` with no-flux boundary conditions. Details about the used meshes and parameters are given in the figure captions.

Traveling burst

Conditions of Theorem 1 provides a constructive way to chose bifurcation and unfolding parameters as well as time constants in (1) to observe traveling bursting waves. Figure 8 shows the result of the numerical integration for $D_w = D_z = 0$.

Figure 9 shows simulation for non-zero D_w and D_z . The simulations support the prediction of Section 8.1, that is, it is the ratio between time-scale separation and space-scale separation that determines the stability of the traveling bursting wave. When this ratio is small, that is, time-scale

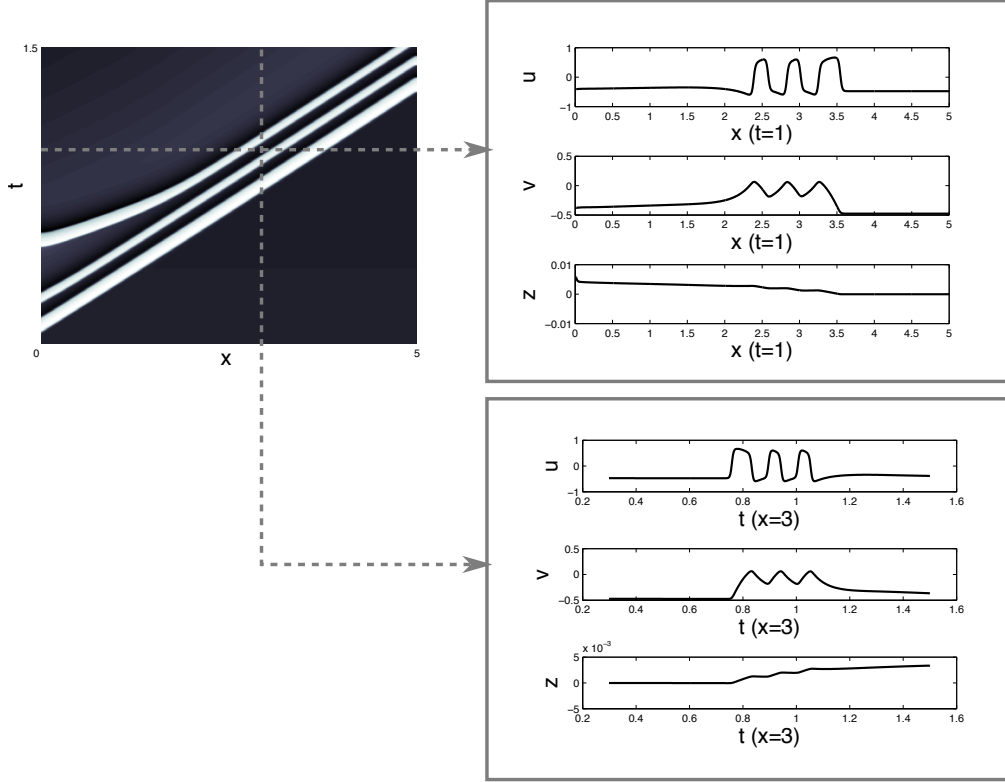


Figure 8: Space mesh: $[0 : 5/3000 : 5]$, time mesh: $[0 : 5/1000 : 5]$. Time constants: $\tau_u = 0.001$, $\tau_w = 0.1$, $\tau_z = 60$. Diffusion constants: $D_u = 0.00005$, $D_w = 0.0$, $D_z = 0.0$. Parameters: $\beta = 1/3$, $\gamma = \gamma_{PF}(\beta)$, $\lambda = \lambda_{PF}(\beta) - 0.02$, $\alpha = \alpha_{PF}(\beta) + 0.47$, where the functions $\lambda_{PF}(\cdot)$, $\alpha_{PF}(\cdot)$, $\gamma_{PF}(\cdot)$ are defined in [1, Appendix A]. The traveling burst was elicited by perturbing the homogeneous resting state with a perturbation $Pert(t, x) = I_{\{0 < x < 0.05\}} I_{\{0 < t < 0.25\}}$, where $I_{\{t\}}$ is the indicator function.

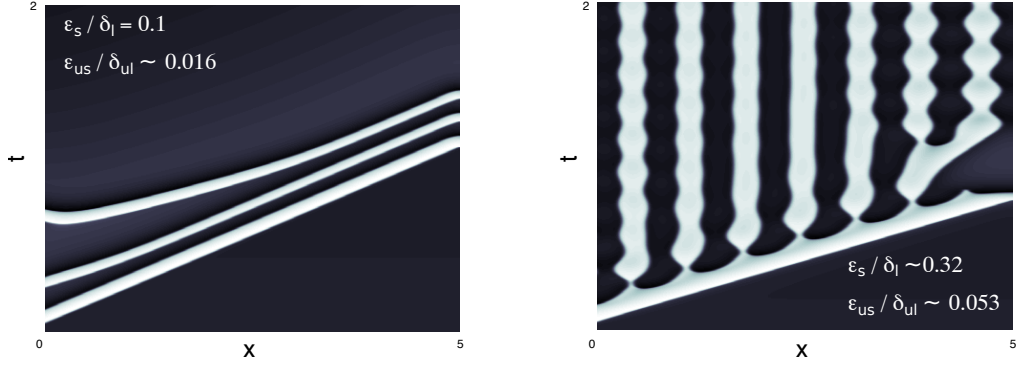


Figure 9: Same parameters as Figure 8 except $D_w = 0.01, D_z = 1.0$ in the left plot and $D_w = 0.1, D_z = 100.0$ in the right plot.

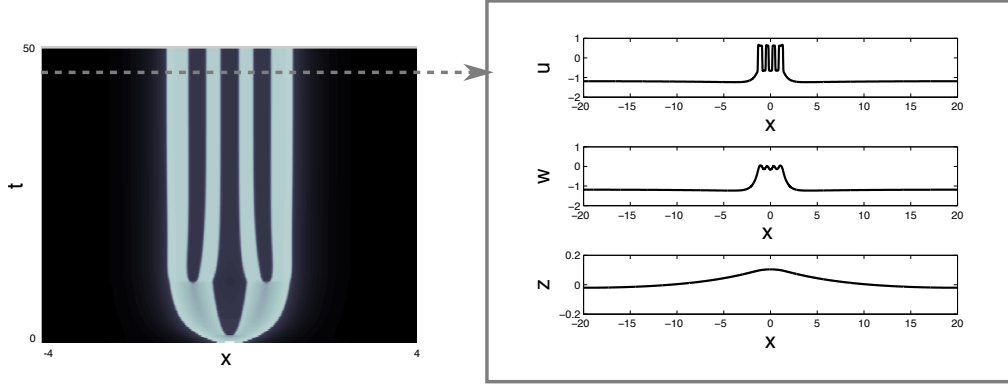


Figure 10: Space mesh: $[-20 : 20/6000 : 20]$, time mesh: $[0 : 50/1000 : 50]$. Time constants: $\tau_u = \tau_w = \tau_z = 0.01$. Diffusion constants: $D_u = 0.0001, D_w = 0.025, D_z = 100$. Parameters: $\beta = 1/3 + 0.1, \gamma = \gamma_{PF}(\beta), \lambda = \lambda_{PF}(\beta) - 0.275, \alpha = \alpha_{PF}(\beta) + 1.125$. The traveling burst was elicited by perturbing the homogeneous resting state with a perturbation $Pert(t, x) = I_{\{-0.1 < x < 0.1\}} I_{\{0 < t < 0.5\}}$

separation dominates space-scale separation, the traveling burst is stable. As this ratio increases and space-scale separation becomes more relevant, the traveling burst loses stability. The resulting pattern exhibits a “breathing” behavior, that is, standing pulses of variable width.

Standing bursts

Conditions of Conjecture 1 provide a constructive way to chose bifurcation and unfolding parameters as well as time constants in (1) to observe traveling bursting waves. Figure 10 shows the result of the numerical integration in the absence of time-scale separation. In line with the singular construction of Section 6.2, $w \sim u$ in the quasi-steady part of the standing burst pattern, whereas only u is at quasi steady state in the oscillatory part.

Figure 11 shows the simulation for increasing time-scale separation. Here again, the numerical simulations support the prediction that it is the dominance of the space-scale separation over the time-scale separation that determines the stability of the standing pulse. For small time-scale separations, the pattern exhibits the same standing burst. Increasing time-scale separation the standing burst

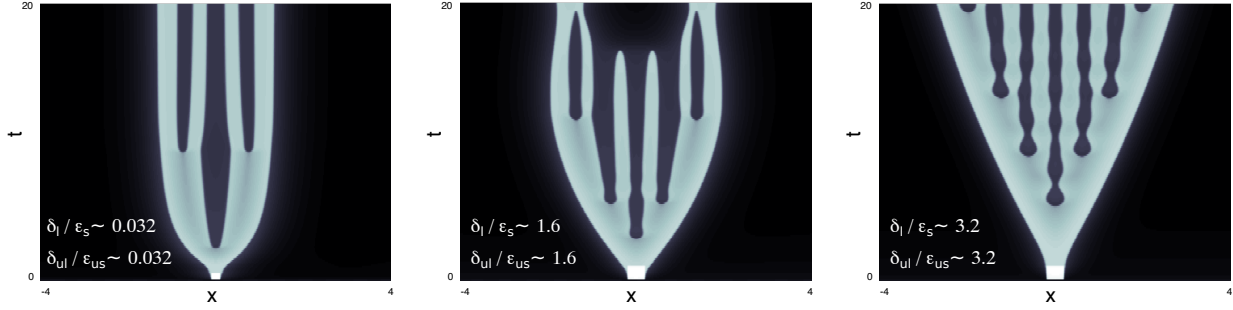


Figure 11: Same parameters as Figure 10 except $\tau_w = 0.1, \tau_z = 1.0$ in the left plot, $\tau_w = 0.5, \tau_z = 25.0$ in the center plot, and $\tau_w = 1.0, \tau_z = 100.0$ in the right plot.

loses stability. For even larger time-scale separation the pattern begins to exhibit the same breathing behavior observed in Figure 9.

8.2 Multi-scale geometric and stability analysis

Beyond the stability analysis, the three-scale model proposed in this paper might motivate an extension of Fenichel theory to more than two scales. To the best of our knowledge, the only effort in this direction can be found in [18]. The reader will notice that the construction of the three-scale standing burst requires two distinct singular limits, in contrast to other multi-scale phenomena that can still be characterized by the classical two-scale theory of Fenichel, such as mixed mode oscillations for instance [19]. The extension of the Exchange Lemma to this class of multi-scale singularly perturbed dynamical systems seems of particular relevance.

Also the problem of stability of the constructed multi-scale spatio-temporal pattern should be addressed carefully and more rigorously. The Evan's function technique was successfully applied in the two-scale scenario both for traveling [3] and standing [6] pulses. An extension to the three-scale scenario might be natural.

A Proof of Theorem 1

We start by a technical lemma that builds a suitable singular skeleton on which we can apply the Exchange Lemma. We refer to Figure 12 for the notation.

Lemma A.1 *Let $\beta = \frac{1}{3}$ and $\gamma = \gamma_{PF}(\frac{1}{3}) = 0$. Let U be a neighborhood of $(\lambda_{PF}(\frac{1}{3}), \alpha_{PF}(\frac{1}{3}))$ in \mathbb{R}^2 . There exists an open set $V \subset U \cap \{\lambda < \lambda_{PF}(\frac{1}{3}), \tilde{\alpha} < \alpha_{PF}(\frac{1}{3})\}$ such that, for all $(\lambda, \tilde{\alpha}) \in V$, the following hold*

- a) For all $c \in \mathbb{R}$, the critical manifold S of (14) has a mirrored hysteresis shape (strong equivalence class 2 of the persistent bifurcation diagrams of the winged cusp listed at [12, page 208]).
- b) Model (14) has exactly three curves of fixed points, corresponding to three roots $u_{rest} < u_o < u_{right}$ of (16). The leftmost curve $\{(u_{rest}, 0, u_{rest}, c), c \in \mathbb{R}\} \subset S_{down}^- \subset S$. The middle one $\{(u_o, 0, u_o, c), c \in \mathbb{R}\} \subset S_{down}^- \cup S_{mid}^- \cup \mathcal{F}_{down}^- \subset S$. The rightmost one $\{(u_{right}, 0, u_{right}, c), c \in \mathbb{R}\} \subset S_{mid}^+ \subset S$. Moreover, u_{rest} satisfies

$$u_{rest}^3 - \beta u_{rest} - \alpha > -u_{rest}^3 + \beta u_{rest} - \alpha > 0,$$

and

$$u_{rest}^3 - (\beta + 1)u_{rest} + \alpha > 0.$$

- c) Let $d_H(\cdot, \cdot)$ denote the Hausdorff distance. Then

$$d_H(S_{down}^- \cap \{w = u_{rest}\}, S_{mid}^- \cap \{w = u_{rest}\}) < d_H(S_{up} \cap \{w = u_{rest}\}, S_{mid}^- \cap \{w = u_{rest}\}).$$

- d) There exists $c^* \in \mathbb{R}$ such that the layer dynamics

$$u' = v, \tag{A.1a}$$

$$v' = cv - g_{wcusp} \left(u, \lambda + w, \tilde{\alpha}, \frac{1}{3}, 0 \right), \tag{A.1b}$$

$$w' = 0, \tag{A.1c}$$

$$c' = 0, \tag{A.1d}$$

of (14) restricted to the hypersurface $\{c = c^*\}$ has four heteroclinic orbits:

- \mathcal{H}_{up}^- , with base point on the equilibrium $(u_{rest}, 0, u_{rest})$ and landing point on S_{up} ;
- \mathcal{H}_{down}^- , with base point on S_{up} at $(u, w) = (-u_{rest}, 0, -\lambda - \sqrt{u_{rest}^3 - \beta u_{rest} - \tilde{\alpha}})$ and landing point on S_{down} ;
- \mathcal{H}_{up}^+ and \mathcal{H}_{down}^+ , which are obtained by symmetry of the layer dynamics with respect to the hypersurface $\{w = -\lambda\}$.

Let \bar{S}_{up} and \bar{S}_{down}^+ be compact, connected, normally hyperbolic submanifolds of S_{up} and S_{down}^+ , respectively, that contain all the base and landing points of the heteroclinic orbits. Then \mathcal{H}_{up}^- is ob-

tained as the transverse intersection (in the (u, v, w, c) space) of the 2-dimensional unstable manifold W_{rest}^u of the curve of fixed points $\{(u_{rest}, 0, u_{rest}, c), c \text{ near } c^*\}$ with the 3-dimensional stable manifold $W^s(\bar{S}_{up})$. The heteroclinic orbits \mathcal{H}_{down}^- , \mathcal{H}_{up}^+ , \mathcal{H}_{down}^+ are obtained as the transverse intersection (in the (u, v, w, c) space) of the 2-dimensional unstable manifold $W^u(\bar{S}_{base}|_{c=c^*})$ of the invariant manifold \bar{S}_{base} containing the base points restricted to the hypersurface $\{c = c^*\}$ with the 3-dimensional stable manifold $W^s(\bar{S}_{land})$ of the invariant manifold \bar{S}_{land} containing the landing points.

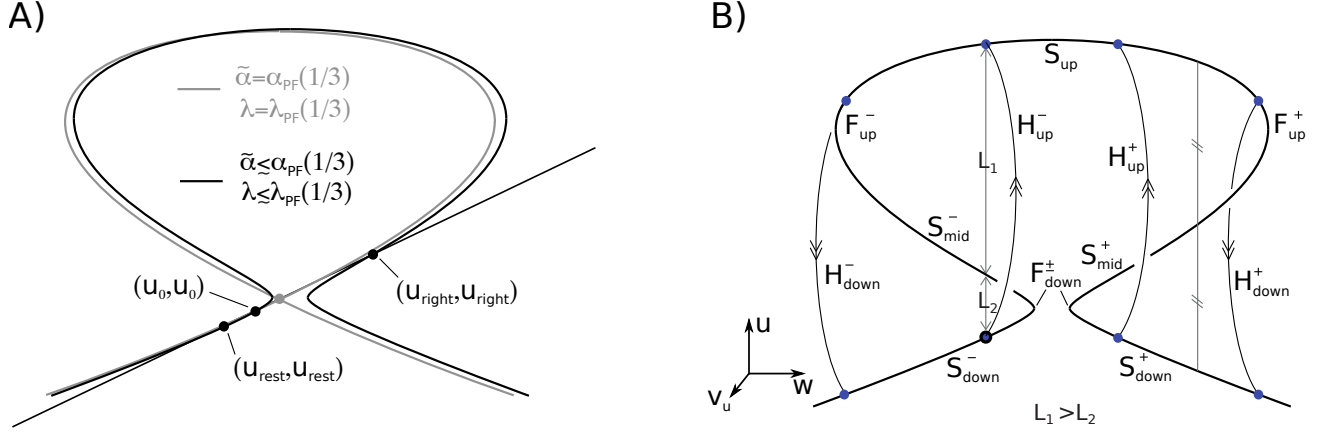


Figure 12: **Geometric construction of the singular phase portrait in Figure 3-A.** Left: critical manifold and fixed points at the pitchfork singularity (gray) and for λ and α satisfying the conditions of Lemma A.1 (black). Right: heteroclinic orbits of the layer dynamics and the different invariant manifolds involved in their construction. $\mathcal{F}_{down}^{+/-}$ and $\mathcal{F}_{up}^{+/-}$ denotes the four fold singularities in the mirrored hysteresis persistent bifurcation diagram. $S_{down}^{+/-}$, $S_{mid}^{+/-}$, and S_{up} are the disconnected open submanifold of S , such that $\mathcal{F}_{down}^{+/-} \cup \mathcal{F}_{up}^{+/-} \cup S_{mid}^{+/-} \cup S_{up} = S$. L_1 and L_2 denotes the distances $d_H(S_{up} \cap \{w = u_{rest}\}, S_{mid}^- \cap \{w = u_{rest}\})$ and $d_H(S_{down}^- \cap \{w = u_{rest}\}, S_{mid}^- \cap \{w = u_{rest}\})$, respectively.

Proof of Lemma A.1. Points $a)$, $b)$, and $c)$ follow from phase plane analysis (Figure 12) quantitatively supported by the inspection of transition varieties and persistent bifurcation diagrams of the critical manifold ($g_{wcusp}(u, \lambda, \tilde{\alpha}, \beta, \gamma) = 0$) and fixed point (16) equations of (14), both cubic universal unfolding of the winged cusp, near the singularity at $(u, \lambda, \tilde{\alpha}, \beta, \gamma) = (-\frac{1}{3}, \frac{1}{3}, -\frac{2}{27}, \frac{1}{3}, 0)$. This singularity is transcritical for the critical manifold equation and pitchfork for the fixed point equation. For the algebraic expressions of the transition and bifurcation varieties, see [12, Page 206] for the critical manifold equation and [1] for the fixed point equation.

To prove $d)$ we use existing results on the FitzHugh-Nagumo traveling pulse equation [5, Sections 4.2 and 5.3]. Points $a-c)$ imply that there exists a diagonal diffeomorphism from a neighborhood of the hypersurface $\{w = u_{rest}\}$ to a neighborhood of the hypersurface $\{w = 0\}$, which is the identity on v and is affine in u , and which maps the layer dynamics (A.1) to the layer dynamics of the FitzHugh-

Nagumo traveling pulse equation [5, Eq. (4.2)] with parameter $0 < a < 1/2$ given by

$$a = \frac{d_H(S_{down}^- \cap \{w = u_{rest}\}, S_{mid}^- \cap \{w = u_{rest}\})}{d_H(S_{up} \cap \{w = u_{rest}\}, S_{down}^- \cap \{w = u_{rest}\})}.$$

Explicitly, the diffeomorphism is given by

$$\begin{pmatrix} u \\ v \\ w \\ c \end{pmatrix} \mapsto \begin{pmatrix} Cu + u_{rest} \\ v \\ -\sqrt{w - u_{rest}^3 + \beta u_{rest} - \alpha} - \lambda \\ c \end{pmatrix}, \quad (\text{A.2})$$

where C is a scaling factor such that $u = 1$ is the largest of the three roots of transformed layer dynamics fixed point equation computed at $w = 0$, that is, $-(Cu + u_{rest})^3 + \frac{1}{3}(Cu + u_{rest}) - (u_{rest} + \lambda)^2 - \alpha = 0$. The smallest root is by construction at $u = 0$ and, by c), the middle root is $u = a$ with $0 < a < 1/2$. Because by b) $-u_{rest}^3 + \beta u_{rest} - \alpha > 0$, the diffeomorphism is well defined.

We now invoke the fact that (A.2) is diagonal, its affine dependence on u , and the fact that it is the identity on v and c . By the chain rule, these properties implies that the differential forms that we use to track invariant manifolds of (A.1) and their intersections are given by linear scaling of the same computations as in the classical FitzHugh-Nagumo equation [5, Section 4.5]. As for the classical FitzHugh-Nagumo equation, we conclude the existence of $c^* \neq 0$ such that (A.1) possesses for $c = c^*$ the heteroclinic orbit \mathcal{H}_{up}^- satisfying the transversality conditions of point d).

Existence of the heteroclinic orbits \mathcal{H}_{down}^- , \mathcal{H}_{up}^+ , and \mathcal{H}_{down}^+ , and their transversality properties follow again from local equivalence of (A.1) with the layer dynamics of the FitzHugh-Nagumo traveling pulse equation [5, Equation (4.2)] and by following the same construction as in [5, Section 5.3].

□

To prove the theorem, we track the 2-dimensional unstable manifold W_{rest}^u of the curve of fixed points $\{(u_{rest}, 0, u_{rest}, c), c \text{ near } c^*\}$, that is, we follow the mapping of a germ of W_{rest}^u through the flow associated to (14). For $\varepsilon > 0$ and sufficiently small, let $\bar{S}_{up,\varepsilon}$ and $\bar{S}_{down,\varepsilon}^+$ be the slow manifolds obtained as Fenichel perturbation of \bar{S}_{up} and \bar{S}_{down}^+ , respectively. Thanks to Lemma A.1d), we can apply [16, Lemma 4.1] and the Exchange Lemma and follow the same arguments as the last two paragraphs of the proof of the Theorem in [16, Section 4] to conclude the following: W_{rest}^u intersects

transversely $W^s(\bar{S}_{up,\varepsilon})$ along \mathcal{H}_{up}^- ; between \mathcal{H}_{up}^- and \mathcal{H}_{down}^+ it lies $\mathcal{O}(\varepsilon)$ -close to S_{up} . It leaves S_{up} along \mathcal{H}_{down}^+ intersecting transversely $W^s(\bar{S}_{down,\varepsilon}^+)$. Between \mathcal{H}_{down}^+ and \mathcal{H}_{up}^+ it lies $\mathcal{O}(\varepsilon)$ -close to S_{down}^+ ; finally, it leaves S_{down}^+ along \mathcal{H}_{up}^+ , again, intersecting transversely $W^s(\bar{S}_{up,\varepsilon})$. We can continue to track the forward mapping of W_{rest}^u through the flow associate to (14) to conclude that it transversely intersects $W^s(\bar{S}_{up,\varepsilon})$ and $W^s(\bar{S}_{down,\varepsilon}^+)$ infinitely many times. Since c is a parameter, all the (one-dimensional) transverse intersections are in the same $\{c = \bar{c}\}$ -slice, for some $\bar{c} = c^* + \mathcal{O}(\varepsilon)$. We claim that the trajectory containing all the transverse intersections, call it h_ε , is the heteroclinic trajectory corresponding to the traveling front.

It remains to show that, in the same $\{c = \bar{c}\}$ -slice there also exists a periodic solution ℓ_ε of (14) and that $h_\varepsilon \subset W^s(\ell_\varepsilon)$. To this aim, we track the two-dimensional unstable manifold $W^u(\bar{S}_{up,\varepsilon}|_{c=\bar{c}})$. By the Exchange Lemma, $W^u(\bar{S}_{up,\varepsilon}|_{c=\bar{c}})$ and W_{rest}^u are $\mathcal{O}(\varepsilon)$ - C^1 close to each other at the heteroclinic jump \mathcal{H}_{down}^+ . It follows that, for ε sufficiently small, also $W^u(\bar{S}_{up,\varepsilon}|_{c=\bar{c}})$ comes back (under the flow associated to (14)) in a neighborhood of S_{up} transversely intersecting $W^s(\bar{S}_{up,\varepsilon})$ inside $\{c = \bar{c}\}$. It follows that the 1-dimensional transverse (in the (u, v, w, c) space) intersection $W^u(\bar{S}_{up,\varepsilon}|_{c=\bar{c}}) \cap_T W^s(\bar{S}_{up,\varepsilon})$ defines a periodic orbit ℓ_ε of (14) in the slice $c = \bar{c}$. Because $W^s(\ell_\varepsilon) = W^s(\bar{S}_{up,\varepsilon}|_{c=\bar{c}})$ and $h_\varepsilon \subset W^s(\bar{S}_{up,\varepsilon}|_{c=\bar{c}})$, the statement is proved for $\beta = 1/3$ and $\gamma = 0$. For $\beta \neq 1/3$, $\gamma \neq 0$, the theorem follows from the persistence of all the transverse intersections used in the construction to arbitrary C^1 perturbations. \square

B Proof of Theorem 2

We use two technical lemmas to build a suitable singular skeleton on which we can apply the Exchange Lemma.

Lemma B.1 *Let $\beta = \frac{1}{3}$ and $\gamma = \gamma_{PF}(\frac{1}{3}) = 0$. For all $\tilde{\alpha} \in [\alpha_{PF}(1/3), 0)$ and all $\lambda \in \mathbb{R}$, the layer dynamics of (15)*

$$u' = v_u, \tag{B.1a}$$

$$v'_u = -g_{wcusp}(u, \lambda + w, \tilde{\alpha}, \frac{1}{3}, 0), \tag{B.1b}$$

possess two heteroclinic orbits at $w = w_{h_1}(\tilde{\alpha})$ and two heteroclinic orbits at $w = w_{h_2}(\tilde{\alpha})$, with $w_{h_1}(\tilde{\alpha}) = -\lambda - \sqrt{-\tilde{\alpha}} < -\lambda < -\lambda + \sqrt{-\tilde{\alpha}} = w_{h_2}(\tilde{\alpha})$. For $\tilde{\alpha} = 0$, model (B.1) possesses two heteroclinic orbits at

$$w = -\lambda.$$

Proof of Lemma B.1. For $w = w_{h_1}(\tilde{\alpha})$ or $w = w_{h_2}(\tilde{\alpha})$, equation (B.1) reduces to

$$u' = v_u, \tag{B.2}$$

$$v'_u = -u^3 + \frac{u}{3}, \tag{B.3}$$

which is Hamiltonian, has three fixed point at $v_u = 0$ and $u = -\frac{1}{\sqrt{3}}, 0, \frac{1}{\sqrt{3}}$ and satisfies

$$\int_{-\frac{1}{\sqrt{3}}}^{\frac{1}{\sqrt{3}}} \left(-u^3 + \frac{u}{3}\right) du = 0$$

□

The notation in the next lemma is defined in Figure 13.

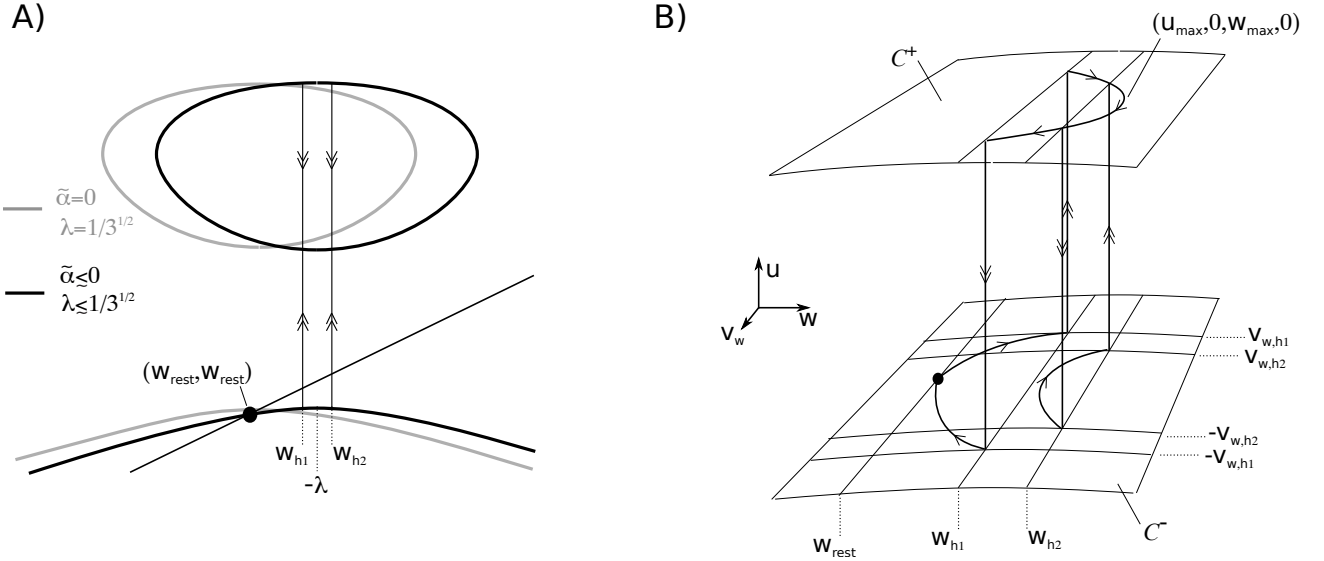


Figure 13: Geometric construction of the singular phase portrait in Figure 3-B.

Lemma B.2 Let $\beta = \frac{1}{3}$ and $\gamma = \gamma_{PF}(\frac{1}{3}) = 0$. There exist a neighborhood U of $(\lambda, \tilde{\alpha}) = (1/\sqrt{3}, 0)$ and an open set $V \subset U \cap \{\lambda < 1/\sqrt{3}, \tilde{\alpha} < 0\}$, such that, for all $(\lambda, \tilde{\alpha}) \in V$ the following hold:

- a) The critical manifold of model (15) belongs to class 3 of the persistent bifurcation diagrams of the winged cusp [12, page 208]. Let w_{fold} be the w -coordinate of the right fold of the critical manifold. Let $u = u_{down}(w)$ be the function such that the lower branch of the critical manifold $C^- = \{(u, v_u, w, v_w) = (u_{down}(w), 0, w, 0)\}$ and $u_{up}(w)$ the function such that the upper branch of the critical manifold between the two fold singularities $C^+ = \{(u, v_u, w, v_w) = (u_{up}(w), 0, w, 0)\}$.

b) Model (15) has a unique fixed point at $(w_{rest}, 0, w_{rest}, 0)$, with $w_{rest} < -\lambda$.

c) The following inequalities hold:

$$\int_{w_{rest}}^{w_{h_1}} (u_{down}(s) - s) ds + \int_{w_{h_1}}^{w_{fold}} (u_{up}(s) - s) ds > 0 \quad (\text{B.4a})$$

$$\int_{w_{rest}}^{w_{h_1}} (u_{down}(s) - s) ds + \int_{w_{h_1}}^{w_{h_2}} (u_{up}(s) - s) ds < 0 \quad (\text{B.4b})$$

Proof of Lemma B.2. Points a), b) follow from phase plane analysis (Figure 13) quantitatively supported by the inspection of transition varieties and persistent bifurcation diagrams of the critical manifold ($g_{wcusp}(u, \lambda, \tilde{\alpha}, \beta, \gamma) = 0$) and fixed point (16) equations of (14), both cubic universal unfolding of the winged cusp, near the singularity at $(u, \lambda, \tilde{\alpha}, \beta, \gamma) = (x_{PF}(\frac{1}{3}), \lambda_{PF}(\frac{1}{3}), \alpha_{PF}(\frac{1}{3}), 1/3, \gamma_{PF}(\frac{1}{3})) = (-\frac{1}{3}, \frac{1}{3}, -\frac{2}{27}, \frac{1}{3}, 0)$. This singularity is transcritical for the critical manifold equation and pitchfork for the fixed point equation. For the algebraic expressions of the transition and bifurcation varieties, see [12, Page 206] for the critical manifold equation and [1] for the fixed point equation.

Point c). Because $\int_{w_{h_1}}^{w_{fold}} (u_{up}(s) - s) ds > 0$ and $w_{rest} = w_{h_1}$ for $(\lambda, \tilde{\alpha}) = (1/\sqrt{3}, 0)$, it follows that (B.4a) is satisfied for $(\lambda, \tilde{\alpha}) = (1/\sqrt{3}, 0)$. By continuity of the integral operator, the same holds true for $(\lambda, \tilde{\alpha})$ sufficiently close to $(1/\sqrt{3}, 0)$.

To prove the second inequality, observe that $\int_{w_{rest}}^{w_{h_1}} (u_{down}(s) - s) ds < 0$ and $w_{h_1} = w_{h_2}$, for $\lambda < 1/\sqrt{3}$ and $\tilde{\alpha} = 0$. Therefore (B.4b) is satisfied for $\lambda < 1/\sqrt{3}$ and $\tilde{\alpha} = 0$. By continuity, the same holds for $(\lambda, \tilde{\alpha})$ sufficiently close to $(1/\sqrt{3}, 0)$. \square

The existence of the homoclinic orbit now follow exactly as [6, Sections 4 and 5]. The two models share indeed the exact same geometry (compare Figure 13 right and [6, Figure 4]). The sole difference is the absence of a fixed point on \mathcal{C}^+ . This only changes the construction of the slow portion of the singular homoclinic orbit on \mathcal{C}^+ . Construction of this portion here follows the same line as in [4, pages 238 and 239].

The same construction is used for the periodic orbit. The only difference is that the initial slow portion is now defined as the slow trajectory passing through the point (w_{h_2}, v_{w,h_2}) instead as the unstable manifold of the fixed point. Then, all the results of [6, Sections 4 and 5] still hold.

The fact that the homoclinic and singular periodic orbits are $\mathcal{O}(\delta_l)$ -close to each other near the point $(u_{max}, 0, w_{max}, 0)$ where w reaches its maximum along the homoclinic trajectory follows from the fact that, near \mathcal{C}^+ , the homoclinic and the periodic orbits are perturbation of, and hence $\mathcal{O}(\delta_l)$ -close to, the same invariant manifold; likewise, for their stable and unstable manifolds.

C Proof of Theorem 3

We refer the reader to Figure 14 for the notation used in the following lemma.

Lemma C.1 *Let $\beta = \frac{1}{3}$ and $\gamma = \gamma_{PF}(\frac{1}{3}) = 0$. Let $V \in \mathbb{R}^2$ and $c^* \neq 0$ be defined as in the statement of Lemma A.1. For all $(\lambda, \alpha) \in V$, the following hold true*

a) *There exists $\Delta\alpha^* > 0$ and $\delta > 0$ such that, for all $\tilde{\alpha} \in [\alpha - \delta, \alpha + \Delta\alpha^*]$ the layer dynamics*

$$u' = v, \tag{C.1a}$$

$$v' = cv - g_{\text{wcusp}} \left(u, \lambda + w, \tilde{\alpha}, \frac{1}{3}, 0 \right), \tag{C.1b}$$

$$w' = 0, \tag{C.1c}$$

$$c' = 0, \tag{C.1d}$$

of (14) restricted to the hypersurface $\{c = c^*\}$ has four heteroclinic orbits $\tilde{\alpha}\mathcal{H}_{\text{up/down}}^{+/-}$ that are all obtained as the transverse intersections (in the (u, v, w, c) space) of the 2-dimensional unstable manifold W^u ($\tilde{\alpha}\bar{S}_{\text{base}}|_{c=c^*}$) of the invariant manifold $\tilde{\alpha}\bar{S}_{\text{base}}$ where the base point lies restricted to the hypersurface $\{c = c^*\}$ with the 3-dimensional stable manifold W^s ($\tilde{\alpha}\bar{S}_{\text{land}}$) of the invariant manifold $\tilde{\alpha}\bar{S}_{\text{land}}$ where the landing point lies².

b) *For $\tilde{\alpha} = \alpha + \Delta\alpha^*$ the two heteroclinic orbits $\tilde{\alpha}\mathcal{H}_{\text{up/down}}^{+/-}$ merge in a fast heteroclinic jump $\mathcal{H}_{\text{up}}^0$. This heteroclinic lies in the hypersurface $\{w = -\lambda\}$ and is obtained as the non-transverse intersection W^u ($\tilde{\alpha}\bar{S}_{\text{down}}|_{c=c^*}$) \cap W^s ($\tilde{\alpha}\bar{S}_{\text{up}}$).*

c) *The two downward heteroclinic jumps $\tilde{\alpha}\mathcal{H}_{\text{down}}^{+/-}$ persist for $\tilde{\alpha} \in [\alpha + \Delta\alpha^*, \alpha + \Delta\alpha^* + \delta)$ and with the same transversality properties as in a).*

d) *For all $\tilde{\alpha} \in [\alpha, \alpha + \Delta\alpha^*]$, let $\tilde{\alpha}w_{\text{up}} < \tilde{\alpha}w_{\text{down}}$ be the w -coordinate of the heteroclinic $\tilde{\alpha}\mathcal{H}_{\text{up}}^+$ and $\tilde{\alpha}\mathcal{H}_{\text{down}}^+$, respectively. There exists $C > 0$ such that, for all $\tilde{\alpha} \in [\alpha, \alpha_{PF}(1/3)]$,*

$$\int_{\tilde{\alpha}w_{\text{up}}}^{\tilde{\alpha}w_{\text{down}}} (u|_{\tilde{\alpha}S_{\text{down}}^+} - (\tilde{\alpha} - \alpha))dw + \int_{\tilde{\alpha}w_{\text{up}}}^{\tilde{\alpha}w_{\text{down}}} (u|_{\tilde{\alpha}S_{\text{up}}} - (\tilde{\alpha} - \alpha))dw > C$$

²As in Lemma A.1, the overline means a compact, connected, normally hyperbolic submanifold of the relative manifold that contains all the base and landing points of the heteroclinic orbits

and, for all $\tilde{\alpha} \in (\alpha_{PF}(1/3), \alpha + \Delta\alpha^*)$,

$$\int_{\tilde{\alpha}w_{up}}^{\tilde{\alpha}w_{down}} (u|_{\tilde{\alpha}S_{down}} - (\tilde{\alpha} - \alpha))dw + \int_{\tilde{\alpha}w_{up}}^{\tilde{\alpha}w_{down}} (u|_{\tilde{\alpha}S_{up}} - (\tilde{\alpha} - \alpha))dw > C.$$

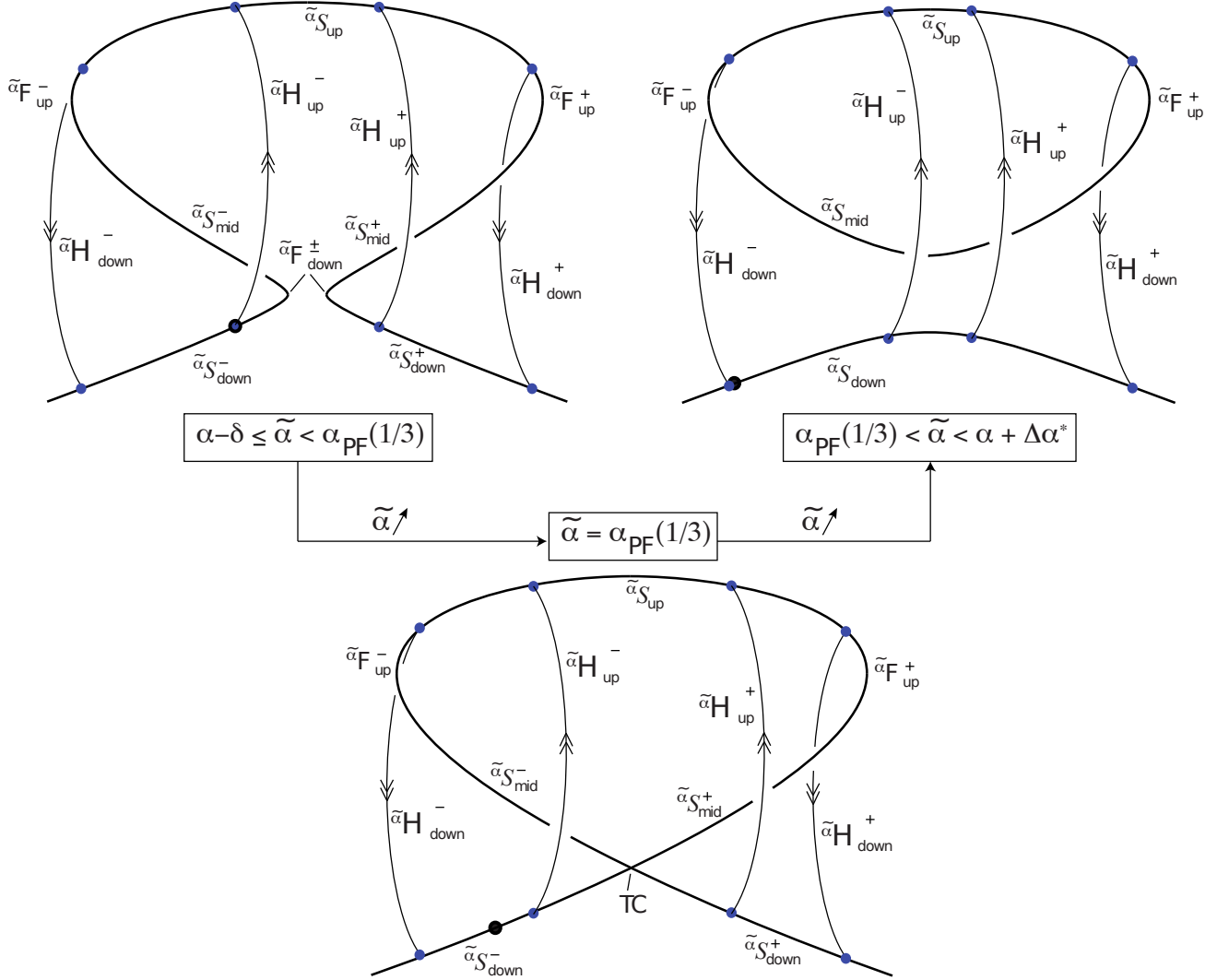


Figure 14

Proof of Lemma C.1.

To prove point *a*) we use again local equivalence to the layer dynamics of the standard FitzHugh-Nagumo pulse equation. The diffeomorphism (A.2) between the layer dynamics (C.1) and the FitzHugh-Nagumo pulse equation [5, Eq. (4.2)] with the same parameter a as above, can be build also for $\tilde{\alpha} \neq \alpha$.

For $\tilde{\alpha}\mathcal{H}_{up}^-$ it reads

$$\begin{pmatrix} u \\ v \\ w \\ c \end{pmatrix} \mapsto \begin{pmatrix} C_{\tilde{\alpha}}u + u_{rest} \\ v \\ -\sqrt{w - u_{rest}^3 + \beta u_{rest} - \tilde{\alpha} - \lambda} \\ c \end{pmatrix},$$

which maps a neighborhood of the hypersurface $\{w = -\sqrt{-u_{rest}^3 + \beta u_{rest} - \tilde{\alpha} - \lambda}\}$ to a neighborhood of $\{w = 0\}$, whereas for $\tilde{\alpha}\mathcal{H}_{down}^-$ it reads

$$\begin{pmatrix} u \\ v \\ w \\ c \end{pmatrix} \mapsto - \begin{pmatrix} C_{\tilde{\alpha}}u - u_{rest} \\ v \\ \sqrt{w + u_{rest}^3 - \beta u_{rest} - \tilde{\alpha} - \lambda} \\ c \end{pmatrix},$$

which maps a neighborhood of the hypersurface $\{w = -\sqrt{u_{rest}^3 - \beta u_{rest} - \tilde{\alpha} - \lambda}\}$ to a neighborhood of $\{w = 0\}$. For $\tilde{\alpha}\mathcal{H}_{up/down}^+$ we use symmetry with respect to the hypersurface $\{w = -\lambda\}$. The w -coordinate of the heteroclinics $\tilde{\alpha}\mathcal{H}_{up}^-$ and $\tilde{\alpha}\mathcal{H}_{down}^-$ are given by $\tilde{\alpha}w_{up}^- = -\sqrt{-u_{rest}^3 + \beta u_{rest} - \tilde{\alpha} - \lambda}$ and $\tilde{\alpha}w_{down}^- = -\sqrt{u_{rest}^3 - \beta u_{rest} - \tilde{\alpha} - \lambda}$, respectively. Their mirrors with respect to the hypersurface $\{w = -\lambda\}$ are $\tilde{\alpha}w_{up}^+ = \sqrt{-u_{rest}^3 + \beta u_{rest} - \tilde{\alpha} - \lambda}$ and $\tilde{\alpha}w_{down}^+ = \sqrt{u_{rest}^3 - \beta u_{rest} - \tilde{\alpha} - \lambda}$. Existence of the four heteroclinic orbits and their transversality conditions then follows as in [5, Section 5.3].

The value $\Delta\alpha^*$ of point b) is computed by imposing $-u_{rest}^3 + \beta u_{rest} - \alpha - \Delta\alpha^* = 0$. As $\tilde{\alpha} \rightarrow \alpha + \Delta\alpha^*$, the two heteroclinics $\tilde{\alpha}\mathcal{H}_{up}^-$ and $\tilde{\alpha}\mathcal{H}_{up}^+$ converge to each other in the Hausdorff distance, because $\lim_{\tilde{\alpha} \rightarrow \alpha + \Delta\alpha^*} \tilde{\alpha}w_{up}^- = \lim_{\tilde{\alpha} \rightarrow \alpha + \Delta\alpha^*} \tilde{\alpha}w_{up}^+ = -\lambda$. For $\tilde{\alpha} = \alpha + \Delta\alpha^*$, the map

$$\begin{pmatrix} u \\ v \\ -\lambda \\ c \end{pmatrix} \mapsto \begin{pmatrix} Cu + u_{rest} \\ v \\ 0 \\ c \end{pmatrix}$$

maps the layer dynamics (C.1) restricted to the hypersurface $\{w = -\lambda\}$ to the traveling wave problem [5, Eq. (4.10)] with the same parameter a as above. With the same computation as [5, Section 4.5], we conclude the existence of the heteroclinic \mathcal{H}_{up}^0 in the same hypersurface $\{c = c^*\}$ as $\tilde{\alpha}\mathcal{H}_{up/down}^{+/-}$, $\alpha \in [\alpha, \alpha + \Delta\alpha)$. The non-transversality condition follows by the fact that transversality is not

compatible with a (local) change in the number of transverse intersections.

By Lemma A.1*b*), we have $u_{rest}^3 - \beta u_{rest} > -u_{rest}^3 + \beta u_{rest}$. This in turn implies that the outer heteroclinics $\mathcal{H}_{down}^{+/-}$ persist and with same properties as in *a*) for $\tilde{\alpha} = \alpha + \Delta\alpha^*$ and, by continuity, also for $\alpha + \Delta\alpha^* < \alpha < \alpha + \Delta\alpha^* + \delta$, which proves *c*).

To prove point *d*), we start by noticing that, by antisymmetry in u of the layer dynamics (A.1), for all $\tilde{\alpha} \in [\alpha, \alpha_{PF}(\frac{1}{3})]$,

$$\int_{\tilde{\alpha}w_{up}}^{\tilde{\alpha}w_{down}} u|_{\tilde{\alpha}S_{down}^+} dw = - \int_{\tilde{\alpha}w_{up}}^{\tilde{\alpha}w_{down}} u|_{\tilde{\alpha}S_{up}} dw$$

and, for all $\tilde{\alpha} \in (\alpha_{PF}(\frac{1}{3}), \alpha + \Delta\alpha^*)$,

$$\int_{\tilde{\alpha}w_{up}}^{\tilde{\alpha}w_{down}} u|_{\tilde{\alpha}S_{down}} dw = - \int_{\tilde{\alpha}w_{up}}^{\tilde{\alpha}w_{down}} u|_{\tilde{\alpha}S_{up}} dw.$$

The proof of *d*) therefore reduces to show that $-u_{rest} - (\tilde{\alpha} - \alpha) > 0$ for all $\tilde{\alpha} \in [\alpha, \alpha + \Delta\alpha^*)$. It suffices to prove this for $\tilde{\alpha} = \alpha + \Delta\alpha^*$. By *b*), $\Delta\alpha^* = -u_{rest}^3 + \beta u_{rest} - \alpha$, so we have to prove that $u_{rest}^3 - (\beta + 1)u_{rest} + \alpha > 0$, which was proved in Lemma A.1*b*). \square

A straightforward corollary of Lemma C.1, obtained by replacing $\tilde{\alpha}$ by $\alpha + z$, is that the singular ($\varepsilon_s = 0$) phase portrait of (6) is as depicted in Figure 4. Let T denote the (2-dimensional) critical manifold of (6). Slices ${}^zT \subset T$ at $z \in [-\delta, \Delta\alpha^* + \delta]$ are given by embedding in \mathbb{R}^5 the critical manifold of (C.1) for $\tilde{\alpha} = \alpha + z$. For each $z \in [0, \Delta\alpha^* + \delta]$ we denote with ${}^zT_{down/up}^{+/-}$ the embedding of $\tilde{\alpha}S_{up/down}^{+/-}$, $\tilde{\alpha} = \alpha + z$, defined as in Figure 14 and, similarly, with ${}^z\tilde{T}_{down/up}^{+/-}$ the embedding of $\tilde{\alpha}\tilde{S}_{up/down}^{+/-}$. For each $z \in [0, \Delta\alpha^* + \delta]$ we denote with ${}^z\mathcal{H}_{up/down}^{+/-}$ and ${}^z\mathcal{H}_{up}^0$ the embedding of $\tilde{\alpha}\mathcal{H}_{up/down}^{+/-}$ and $\tilde{\alpha}\mathcal{H}_{up}^0$, where they exist.

This singular phase portrait provides a skeleton for the application of the theorem in [16, Section 4]. In particular, we can build a singular homoclinic trajectory from the resting point to itself consisting of finitely many jumps along the family of heteroclinic orbits ${}^z\mathcal{H}_{up/down}^{+/-}$ of the layer dynamics of (23) connected slow trajectories of the reduced dynamics (24). This trajectory was sketched in Figure 4. Transversality properties of $\tilde{\alpha}\mathcal{H}_{up/down}^{+/-}$ will translate into the needed transversality condition [16, Eqs. (4.2) and (4.3)].

For the existence of the singular homoclinic trajectory, we invoke Lemma C.1*d*). It implies that for $\frac{\varepsilon_{us}}{\varepsilon_s} > 0$ and sufficiently small and as long as $z < \Delta\alpha^*$, the z -coordinate of two successive jumps-down and of two successive jumps-up is strictly uniformly monotonically increasing (by an amount bounded

from below by $C \frac{\varepsilon_{us}}{\varepsilon_s}$. By continuity, this implies that, generically in the model parameters, the last jump-down happens for $z > \Delta\alpha^*$ and that the subsequent slow motion crosses the hypersurface $\{w = -\lambda\}$ also for $z > \Delta\alpha^*$. Genericity is necessary to avoid the non-transversal heteroclinic \mathcal{H}_{up}^0 existing for $z = \Delta\alpha^*$. The trajectory then converges toward the quasi-steady state of the slow-fast subsystem (6a-6c) and then to rest.

We now verify the two transversality conditions [Jones and Koppel, Eqs. (4.2) and (4.3)]. Let

$$T^0 := \bigcup_{z \in [-\delta, \alpha_{PF}(\frac{1}{3}) - \alpha]} ({}^z\bar{T}_{down}^- \cup {}^z\bar{T}_{down}^+) \cup \bigcup_{z \in (\alpha_{PF}(\frac{1}{3}) - \alpha, \Delta\alpha^* + \delta]} {}^z\bar{T}_{down}$$

and

$$T^1 := \bigcup_{z \in [-\delta, \Delta\alpha^* + \delta]} {}^z\bar{T}_{up},$$

that is, T^0 and T^1 are compact, connected, normally hyperbolic (for the layer dynamics of (6) sub-manifolds of the critical manifold T that contains all the base and landing point of the heteroclinic orbits ${}^z\mathcal{H}_{up/down}^{+/-}$, in particular, T^0 contains base points of upward heteroclinic and landing points of downward heteroclinic, and viceversa for T^1).

To verify [16, Eq. (4.2)], we have to prove that, in the layer dynamics of (6), that is, for $\varepsilon = 0$, the first heteroclinic jump of the singular homoclinic trajectory, along ${}^0\mathcal{H}_{up}^-$ is obtained as the transverse intersection $W_{rest}^u \cap_T W^s(T^1)$, where W_{rest}^u is the 2-dimensional unstable manifold of the line of fixed points $\{(u_{rest}, 0, u_{rest}, c, 0), c \text{ near } c^*\}$, whereas $W^s(T^1)$ is 4-dimensional. Note that $W_{rest}^u \subset \{z = 0\}$ and that $W^s(T^1) \cap \{z = 0\} = W^s(S^{up})$, where S^{up} is defined as in Lemma A.1. It follows by Lemma A.1d) that $W_{rest}^u \cap_T W^s(T^1)$ inside $\{z = 0\}$. Since the full space only adds the z -direction, $W_{rest}^u \cap_T W^s(T^1)$, which verifies [16, Eq. (4.2)] for (6).

Next, we verify [16, Eqs. (4.3)] for all successive jumps. We write the condition explicitly for the first jump down along ${}^{z^*}\mathcal{H}_{down}^+$ for some $z^* > 0$. Computations for other jumps are similar and therefore omitted. We have to verify that $W^u(T^1|_{sing.orbit}) \cap_T W^s(T^0)$. First, we note that the singular homoclinic trajectory is in the hypersurface $\{c = c^*\}$. Second, as $\varepsilon_z \rightarrow 0$, the slow motion after the first jump-up converges in the Hausdorff distance to the hypersurface $\{z = 0\}$, that is, $\lim_{\varepsilon \rightarrow 0} T^1|_{sing.orbit} = T^1|_{c=c^*, z=0}$, where the limit is again in the Hausdorff distance. Since $W^u(T^1|_{c=c^*, z=0}) \subset \{z = 0\}$, reasoning as above we can invoke Lemma A.1d) to conclude that $W^u(T^1|_{c=c^*, z=0}) \cap_T W^s(T^0)$ inside the subspace $\{z = 0\}$ and therefore, by adding the z -dimension, in

the whole space. Because $W^u(T^1|_{\text{sing.orbit}})$ is $O(\varepsilon_z)$ -close to $W^u(T^1|_{c=c^*,z=0})$, for ε_z sufficiently small also $W^u(T^1|_{\text{sing.orbit}}) \cap_T W^s(T^0)$.

We can now apply the theorem in [16, Section 4] to conclude that, for $\varepsilon > 0$ sufficiently small, there exists a unique homoclinic solution of (6), which proves the statement of the theorem for $\beta = 1/3$ and $\gamma = 0$. For $\beta \neq 1/3$ and $\gamma \neq 0$, the statement follows from the persistence of transverse intersections to arbitrary C^1 perturbations. \square

References

- [1] A. Franci, G. Drion, and R. Sepulchre. Modeling the modulation of neuronal bursting: a singularity theory approach. *SIAM Journal on Applied Dynamical Systems*, 13(2):798–829, 2014.
- [2] G. A. Carpenter. A geometric approach to singular perturbation problems with applications to nerve impulse equations. *Journal of Differential Equations*, 23(3):335–367, 1977.
- [3] C. K. R. T. Jones. Stability of the travelling wave solution of the fitzhugh-nagumo system. *Transactions of the American Mathematical Society*, 286(2):431–469, 1984.
- [4] J. D. Dockery. Existence of standing pulse solutions for an excitable activator-inhibitory system. *Journal of Dynamics and Differential Equations*, 4(2):231–257, 1992.
- [5] C.K.R. Jones. Geometric singular perturbation theory. In *Dynamical systems. Springer Lecture Notes in Math. 1609*, pages 44–120, Berlin, 1995. Springer.
- [6] C. K. R. T. Jones and J. E. Rubin. Existence of standing pulse solutions to an inhomogeneous reaction–diffusion system. *Journal of Dynamics and Differential Equations*, 10(1):1–35, 1998.
- [7] E. Maeda, H. P. Robinson, and A. Kawana. The mechanisms of generation and propagation of synchronized bursting in developing networks of cortical neurons. *The Journal of neuroscience*, 15(10):6834–6845, 1995.
- [8] D. Golomb and Y. Amitai. Propagating neuronal discharges in neocortical slices: computational and experimental study. *Journal of neurophysiology*, 78(3):1199–1211, 1997.
- [9] S. A. Newman and H. L. Frisch. Dynamics of skeletal pattern formation in developing chick limb. *Science*, 205(4407):662–668, 1979.
- [10] A. Doelman, P. Van Heijster, and T. J. Kaper. Pulse dynamics in a three-component system: existence analysis. *Journal of Dynamics and Differential Equations*, 21(1):73–115, 2009.

- [11] B. Ermentrout and D. H. Terman. *Foundations of mathematical neuroscience*. Citeseer, 2010.
- [12] M. Golubitsky and D. G. Schaeffer. Singularities and groups in bifurcation theory. *Appl. Math. Sci*, 51, 1985.
- [13] A. Franci, G. Drion, and R. Sepulchre. An organizing center in a planar model of neuronal excitability. *SIAM Journal on Applied Dynamical Systems*, 11(4):1698–1722, 2012.
- [14] R. FitzHugh. Impulses and physiological states in theoretical models of nerve membrane. *Biophysical journal*, 1(6):445, 1961.
- [15] N. Fenichel. Geometric singular perturbation theory for ordinary differential equations. *Journal of Differential Equations*, 31(1):53–98, 1979.
- [16] C. K. R. T. Jones and N. Kopell. Tracking invariant manifolds with differential forms in singularly perturbed systems. *Journal of Differential Equations*, 108(1):64–88, 1994.
- [17] J. E. Rubin. Stability, bifurcations and edge oscillations in standing pulse solutions to an inhomogeneous reaction-diffusion system. *Proceedings of the Royal Society of Edinburgh: Section A Mathematics*, 129(05):1033–1079, 1999.
- [18] P. Cardin, P. da Silva, and M. Teixeira. Three time scale singular perturbation problems and nonsmooth dynamical systems. *Quarterly of Applied Mathematics*, 72(4):673–687, 2014.
- [19] M. Desroches, J. Guckenheimer, B. Krauskopf, C. Kuehn, H. M. Osinga, and M. Wechselberger. Mixed-mode oscillations with multiple time scales. *SIAM Review*, 54(2):211–288, 2012.